NASA TECHNICAL MEMORANDUM

NASA TM X-3062

NASA TM X-3062

LOW-SPEED WIND TUNNEL TESTS OF A 50.8-CENTIMETER (20-IN.) 1.15-PRESSURE-RATIO FAN ENGINE MODEL

by Howard L. Wesoky, John M. Abbott, James A. Albers, and Donald A. Dietrich

Lewis Research Center
Cleveland, Ohio 44135

NATIONAL AERONAUTICS AND SPACE ADMINISTRATION • WASHINGTON, D. C. • JUNE 1974

1. Report No.	2. Government Accession No.	3. Recipient's Catalog No.
NASA TM X-3062		

4. Title and Subtitle	5. Report Date
LOW-SPEED WIND TUNNEL TESTS OF A 50.8-CENTIMETER (20-IN.) 1.15-PRESSURE-RATIO FAN ENGINE MODEL	JUNE 1974
	6. Performing Organization Code

7. Author(s)	8. Performing Organization Report No.
Howard L. Wesoky, John M. Abbott, James A. Albers, and Donald A. Dietrich	E-7844
	10. Work Unit No. 501-24
9. Performing Organization Name and Address Lewis Research Center National Aeronautics and Space Administration Cleveland, Ohio 44135	11. Contract or Grant No.
	13. Type of Report and Period Covered Technical Memorandum
12. Sponsoring Agency Name and Address National Aeronautics and Space Administration Washington, D.C. 20546	14. Sponsoring Agency Code

15. Supplementary Notes

16. Abstract

At a typical STOL aircraft takeoff and landing velocity, wind tunnel aerodynamic and acoustic measurements demonstrated that an inlet lip-area contraction ratio of 1.35 was superior to a ratio of 1.26 at high incidence angles. A 17 percent reduction in net thrust and an increase of 9 decibels in sound pressure level at the blade passing frequency resulted from inlet flow separation at an incidence angle of 50° with the 1.26-contraction-ratio inlet. Reverse-thrust forces obtained with blade rotation through the "feathered" angle were 1.8 times larger than with blade rotation through the "flat" angle. Reverse-thrust force was reduced from 30 to 50 percent and sound pressure level increased from 3 to 7 decibels at the blade passing frequency between the wind-tunnel-off condition and a typical STOL aircraft landing velocity.

17. Key Words (Suggested by Author(s))	18. Distribution Statement
STOL propulsion Fan engine Inlet Reverse thrust	Unclassified - unlimited Category 28

19. Security Classif. (of this report)	20. Security Classif. (of this page)	21. No. of Pages	22. Price*
Unclassified	Unclassified	44	$3.25

* For sale by the National Technical Information Service, Springfield, Virginia 22151

LOW-SPEED WIND TUNNEL TESTS OF A 50.8-CENTIMETER (20-IN.) 1.15-PRESSURE-RATIO FAN ENGINE MODEL

by Howard L. Wesoky, John M. Abbott, James A. Albers, and Donald A. Dietrich

Lewis Research Center

SUMMARY

A model aircraft engine with a 50.8-centimeter (20-in.) diameter, 1.15-pressure-ratio fan with a variable-pitch rotor was tested in an isolated nacelle configuration at wind tunnel velocities from 0 to 44 m/sec (143 ft/sec) and at model incidence angles from 0° to 50°. With forward thrust, higher total pressure recovery and less distortion were obtained at high fan speeds and high model incidence angles with an inlet lip-area contraction ratio of 1.35 than with a contraction ratio of 1.26. A 17 percent reduction in net thrust resulted from reduced fan weight flow and stage pressure ratio caused by flow separation at 50° in the low-contraction-ratio inlet. Decreases in aerodynamic performance of the inlet were accompanied by increases in reverberant noise levels of as much as 9 decibels near the blade passing frequency and larger increases over a broad range of lower frequencies.

Reverse-thrust forces obtained with blade rotation through the "feathered" angle were about 1.8 times larger than with blade rotation through the "flat" angle. Reverse-thrust force was reduced from 30 to 50 percent and reverberant noise level increased from 3 to 7 decibels near the blade passing frequency between a wind-tunnel-off condition and a typical STOL aircraft landing velocity.

INTRODUCTION

Interest in the application of very-high-bypass-ratio fan jet engines for short takeoff and landing (STOL) aircraft has led the Lewis Research Center to examine problems of nacelle design and performance related to propulsive lift systems. At takeoff and landing conditions, important areas for experimental research were considered to be the coupled aerodynamic performance of the fan and nacelle at STOL aircraft speeds and incidence angles and the reverse-thrust performance with a variable-pitch rotor. Acous-

tic performance variation with flight speed and nacelle incidence angle, for both forward and reverse thrust, was also considered to be an important area for experimental investigation.

To obtain the necessary data, an engine model with a 50.8-centimeter (20-in.) diameter, 1.15-pressure-ratio fan with a variable-pitch rotor was tested in the Lewis Research Center's 9- by 15-Foot V/STOL Wind Tunnel. Tests were conducted with an isolated nacelle configuration at wind tunnel velocities from 0 to 44 m/sec (143 ft/sec) and at model incidence angles from 0° to 50°. Two inlet cowls having the same external contour but different lip-area contraction ratios were tested with two spinners, providing data for three inlet duct-area distributions. Two fan nozzles differing in exit area by 8 percent were also examined in the wind tunnel tests.

Tests of reverse-thrust performance with no wind tunnel flow were conducted to determine the effect of rotor blade pitch angle. A wind tunnel test also investigated the effect of forward speed on reverse thrust. Reverberant noise levels were measured for both forward and reverse thrust.

SYMBOLS

A	area
BPF	blade passing frequency
D	diameter
DI_{max}	distortion, eq. (1)
DI_{60}	circumferential distortion, eq. (2)
F	model fan net axial thrust
l	nozzle length
P	pressure
V	velocity
W	fan weight flow
X	axial length
Y	fan nacelle length
Z	model length
α	model incidence angle
γ	fan blade design setting angle

δ ratio of total pressure to standard sea-level pressure

θ ratio of total temperature to standard sea-level temperature

φ maximum cowl diffuser surface angle relative to model axis

Subscripts:

av average

d inlet duct, cowl throat to fan face

e fan nozzle exit

f cowl external forebody

fh fan hub

ft fan tip

max maximum

min minimum

min60 minimum over any 60 degree interval

s spinner

T cowl throat

t total condition

0 tunnel free stream

1 cowl highlight

2 fan face

3 fan stage exit, for duct annulus (fig. 4)

APPARATUS

Fan Model

A schematic drawing of the model, indicating some significant dimensions, is shown in figure 1. Nacelle dimensions given in the figure are for those configurations tested with tunnel flow. Construction of the model permitted changing of the fan rotor and stator for other experiments. The components of the model used in the present experiment are described in the following paragraphs.

Fan stage. - The 50.8-centimeter (20-in.) tip diameter fan stage consisted of 12 rotor blades and 32 stator blades. A constant hub-tip radius ratio of 0.4 existed from

the rotor leading edge to the stator trailing edge. The rotor was designed for a 244-m/sec (800-ft/sec) tip speed, or 9160 rpm, at standard sea-level pressure and temperature. At standard conditions, the design weight flow was 30 kg/sec (66 lbm/sec) and the design total pressure ratio was 1.15. A manual adjustable pitch mechanism allowed setting of the fan rotor blades at any desired angle for forward or reverse thrust. Some aspects of the design which were related to the low pressure ratio and variable pitch were the small number of rotor blades, the low rotor solidity, and the low tip speed. Some details of the fan design are given in figure 2. The large axial spacing between the rotor and stator was used to minimize noise caused by the impingement of the rotor wakes on the stator. Further details of the fan design and performance are provided in reference 1.

Turbine. - The fan was driven by a $4\frac{1}{2}$-stage, 15-centimeter (5.9-in.) diameter turbine which used air as the driving fluid. Reference 2 gives a detailed description of the turbine design and performance. Design turbine inlet temperature was 367 K (660° R), design inlet pressure was 241 N/cm^2 (350 psia), and design weight flow was 5.5 kg/sec (12 lbm/sec). Drive air was delivered to the turbine plenum through the pylon shown in figure 1.

Fan inlets. - Axisymmetric inlets, shown in figure 3, were designed by using empirical information from references 3 to 6. The external forebodies (contours from highlight to maximum nacelle diameter) were designed for a drag divergence Mach number of 0.80 with an equivalent fan weight flow of 34.5 kg/sec (75.9 lbm/sec) at a cruise Mach number of 0.75. A single NACA 1-Series contour (ref. 3) was used for the external forebody of both cowls. The ratio of highlight diameter to maximum cowl diameter D_1/D_{max} was 0.935, and the ratio of length to maximum nacelle diameter X_f/D_{max} was 0.175. Maximum nacelle diameter was chosen to keep the nacelle projected area and the surface area low. The resulting ratio of maximum nacelle diameter to fan diameter, 1.075, was small but would probably be sufficient for a full-scale flight engine.

After the highlight diameter D_1 was specified according to the previous arguments, the maximum lip-area contraction ratio A_1/A_T was chosen so that the highest inlet cowl-throat Mach number would be 0.75, as suggested in reference 4. This restriction resulted in the cowl design with $A_1/A_T = 1.35$ (fig. 3). The other cowl contraction ratio of 1.26 was chosen to be typical of current high-bypass-ratio engines (ref. 4). The lip contours between the cowl highlight and throat were elliptical, with the major axis parallel to the cowl axis and twice the length of the minor axis (ref. 5).

Inlet diffusers were conservatively designed according to references 4 and 5, as shown by the small values of diffuser effective cone angle given in figure 3. These angles resulted from the restriction of the maximum cowl diffuser surface angle to 10°, as suggested by reference 6. Cowl surface contours from the cowl throat to the fan face were third-order polynomials (cubic distribution of radius) with the coefficients deter-

mined from the cowl surface radii and the zero slopes at the throat and fan face. The two spinners (fig. 3) had NACA 1-Series contours (ref. 3) and projected to the throats of each cowl. Thus, the minimum duct area was downstream of the cowl throats for three of the cowl and spinner combinations noted in figure 3, as indicated by the ratios A_1/A_{min} and A_1/A_T.

For some tests of the model with no wind tunnel flow, a standard bellmouth inlet, designed according to the specifications of reference 7, was used for the fan inlet. The throat diameter of the bellmouth inlet was equal to the fan tip diameter, and the length of the throat was extended about 38 centimeters (15 in.) to allow static pressure measurement without interference from the fan spinner. Four static pressure taps and four total pressure tubes were installed in the cylindrical section of the bellmouth inlet.

Fan nozzles. - The two types of fan nozzles used in the experiment can be classified according to the fan thrust direction during their application. Nozzles for forward-thrust application are described in figure 4(a), and the nozzles for reverse-thrust application are described in figure 4(b). The word nozzle is used here only as a matter of convention to describe the fan aft duct. As can be seen from the tabulation of the area ratio A_e/A_3 in figure 4(a), the forward-thrust nozzles were actually diffusers, with varying amounts of area increase between the fan exit and the duct exit. To meet both low flight speed and cruise requirements, a low-pressure-ratio fan may require a variable-area nozzle, but no attempt was made in the present experiment to simulate this requirement. A gradual straight taper was used from near the stator exit to the nozzle exit.

For reverse thrust or reverse fan pitch, the nozzle might better be described as an inlet because of the change in flow direction. The bellmouth nozzle shown in figure 4(b) was used to obtain reverse-thrust data with small inlet losses. The flared nozzle also shown in figure 4(b) was designed to simulate a variable-area conventional nozzle which would open as indicated to reduce lip losses for reverse flow.

Instrumentation

A schematic diagram of the model showing research instrumentation locations and a tabulation of this instrumentation is given in figure 5. A more detailed description of the instrumentation will be given using the zones indicated in figure 5 as a reference. The pitot tubes in all zones were not useful for the reverse-thrust tests because they were directed in the conventional upstream direction.

Zone 1. - Instrumentation of the inlet from the leading edge to the fan face consisted entirely of static pressure taps on the cowl surfaces. The total number of taps for each cowl is given in figure 5. These were distributed in axial rows at various circumferential locations, both on the inside and outside of the cowls. The density of the pressure

taps was highest near the inlet leading edge, or highlight, where the highest pressure gradients were expected. Data to be reported herein are from the windward side of the inside cowl surface.

Zone 2. - At the fan face, instrumentation was installed on a ring which fit between the inlet cowl and the fan casing. Twelve rakes, evenly spaced, were mounted on the ring. Six of these rakes, referred to as flow rakes in figure 5, extended across the fan duct, with each rake having six pitot tubes placed at the centroids of equal areas. The other six rakes, referred to as boundary layer rakes in figure 5, were spaced between the flow rakes. These rakes also each had six pitot tubes which were spaced from 0.076 to 2.82 centimeters (0.030 to 1.11 in.) from the cowl surface. Between the 12 rakes, 12 static pressure taps were evenly spaced around the ring. The axial position of the static pressure taps was the upstream end of the rake pitot tubes. A single total pressure probe containing a fast-response transducer to measure time-dependent pressure fluctuations was mounted 1.27 centimeters (0.50 in.) from the cowl surface, 7.5° from the windward side of the cowl.

Zone 3. - Four pitot tubes were installed in the leading edge of each of four stator blades near the fan hub. Also, a single total pressure probe with a fast-response transducer was installed in the leading edge of each of four other stator blades near the fan hub. Twelve static-pressure taps, evenly divided between the inside and outside of the fan duct annulus, were installed at the same axial position as the upstream ends of the pitot tubes.

Zone 4. - At the fan stage exit, six rakes similar to the flow rakes of zone 2 were installed. The evenly spaced rakes each consisted of six pitot tubes located at the centroids of equal areas and a single total temperature (thermocouple) probe at the centroid of the fan duct annular area. Twelve static pressure taps, evenly divided between the inside and outside of the fan duct annulus, were located between the rake positions. The axial position of the static pressure taps and pitot tubes was 1.78 centimeters (0.70 in.) downstream of the stator trailing edge. To avoid direct impingement of stator wakes, the static pressure taps and rakes were located between circumferential positions of the stator blades.

Zone 5. - Instrumentation in the fan nozzle was located in two axial positions. One location was three stator chord lengths behind the stator trailing edge. At this location, the pitot tube instrumentation was the same as in zone 3. Seven static pressure taps were located around the inside of the fan duct annulus, and three fast-response transducers were installed in total pressure probes near the inside of the annulus. The second axial location was 2.54 centimeters (1 in.) upstream from the exit plane of the forward-thrust nozzles. Six static pressure taps were distributed around the inner wall of the fan duct annulus and a like number around the outer wall. The reverse-thrust nozzles had no instrumentation on the outer wall of the fan duct annulus.

Zone 6. - Four rakes were located 1.27 centimeters (0.5 in.) downstream of the

turbine exit guide vanes, evenly spaced between vanes. Two rakes had two pitot tubes and a single total temperature probe, and the other two rakes had two total temperature probes and a single pitot tube. The pitot tubes and temperature probes were located at the centroids of appropriate areas. Four static pressure taps were located around the outer wall of the turbine flow passage at the same axial location as the rake instruments, and two static pressure taps were located on the inner wall of the flow passage. Six static pressure taps were located on the turbine nozzle boattail, evenly divided between two axial rows near the nozzle exit plane. Instrumentation in this zone was used to measure both the thrust from the turbine nozzle jet and the turbine power output.

Test Facility

The test program was conducted in the NASA Lewis Research Center 9- by 15-Foot V/STOL Wind Tunnel, which is described in reference 8. The model installed in the test section is shown in figure 6. No corrections were made to the force data reported herein to compensate for wind-tunnel-wall interference effects or model blockage.

Model installation. - A schematic drawing of the model installation in the wind tunnel is shown in figure 7. As indicated in both figures 6 and 7, the pylon of the engine model was oriented in a horizontal plane and the model was rotated in this plane. This orientation simulated the pitching motion of an aircraft installation. The pylon was connected to a vertical pipe which supported the model in the wind tunnel and through which drive air was supplied to the turbine. This pipe was attached to the force balance below the tunnel floor, and the force balance was mounted on a motor-driven turntable which provided angular movement for the model. Below the turntable, the air supply flowed through a flexible hose which terminated at a pipe swivel. The flexible hose effectively eliminated transfer of unwanted forces to the balance system through the air-supply piping.

In the wind tunnel test section, an aerodynamic fairing was installed around the vertical air-supply pipe to eliminate aerodynamic forces on that part of the model support. The fairing was mounted on the floor of the test section and did not contact the model or its support. The axisymmetric object, shown in figure 6, at the top of the fairing, served as a transition between the engine pylon and the vertical pipe and was, therefore, connected to the force balance. Instrumentation tubes and wires were led out of the simulator through the pylon and, from the pylon, were attached to the outside of the air-supply pipe.

Force balance. - Forces on the model were measured with an external three-component (axial and normal forces and pitching moment) balance. Two of the three elements of the balance were strain-gage linkages, and the third element was a calibrated load cell. A static calibration of the balance, including application of combined forces

along two axes and pressurization of the air-supply piping, indicated a measurement accuracy of about 3 percent over its full range. The balance rotated with the model, and the axial or thrust force measurement was alined with the fan axis of rotation.

Noise measurements. - Acoustic data were measured with four microphones located in the wind tunnel settling chamber, about 24 meters (80 ft) upstream of the model (fig. 7). Sound pressure levels from the microphones were selectively averaged to minimize any irregularities in the measurement. The hard walls of the wind tunnel approximated a reverberant chamber, eliminating the measurement of directional noise variation. Because of frequency selective attenuation in the reverberant situation, the spectra measured do not correspond to those that would be obtained by far-field measurement. However, the relative changes in level at a given frequency are properly associated with changes in model configuration or test condition.

Data Recording and Analysis Systems

Model research instrumentation data and force balance data were recorded by the Lewis Research Center's Central Automatic Digital Data Encoder and simultaneously recorded and analyzed by a time-sharing digital computer system. The large amount of pressure data was recorded by the digital data encoder using nine automatic scanning valves, each having 48 ports. A computer plotting program was used to prepare the fan face total pressure contours described in the section FORWARD-THRUST RESULTS, and microfilm plots prepared by the computer were used to analyze other results of the experiment. Microphone data were recorded on magnetic tape, and the microphone data reported herein were processed with a 1/3-octave band spectrum analyzer.

PROCEDURE

In this section of the report, the procedure for conducting the test program, the test parameters, and the model configurations are explained. Some results, directly pertaining to these subjects, are discussed here. The general results of the test program are discussed in the sections FORWARD-THRUST RESULTS and REVERSE-THRUST RESULTS. Unless otherwise stated, all test parameters are given at equivalent standard sea-level pressure and temperature conditions.

Forward-Thrust Tests

Tunnel velocity. - All nacelle configurations were tested at three tunnel velocity

levels and also with no wind tunnel flow. The equivalent velocities $V_0/\sqrt{\theta_0}$ were 24, 32, and 43 m/sec (80, 105, and 140 ft/sec). The highest velocity approximates the takeoff and landing speed of a STOL transport designed for a 610-meter (2000-ft) field length, and the next highest approximates STOL takeoff and landing speeds for a 460-meter (1500-ft) field length.

Absolutely static conditions could not be obtained with the wind tunnel drive off because the engine model induced a significant flow in the wind tunnel. Depending on the operating condition, tunnel velocities as high as 13 m/sec (41 ft/sec) were measured. Therefore, the force balance measurements at the nominal static conditions to be discussed include drag forces and inlet momentum forces caused by this induced velocity. The small variation from an actual static condition does not affect the general objectives of the experiment. Tests with the wind tunnel drive system not operating are referred to as "wind tunnel off" tests.

Fan speed. - Data were measured at 70, 90, 100, 110, and 120 percent of the fan equivalent design speed of rotation, which was 9160 rpm. Some data were omitted at the design speed because of a vibration problem in the model encountered only at this speed. Overspeed runs were made because the fan weight flow and total pressure ratio were below the design values at design speed. The fan overspeed achieved the required inlet weight flows corresponding to the design value.

Model incidence angle. - The model incidence angle, which is defined as the angle between the model axis and the tunnel axis (fig. 3), was varied from 0° to 50°. The upper limit was chosen because it has been shown that the effective angle of nacelles mounted on current jet transports can be greater than 40°, and it is expected that the closely coupled wing and engines of an externally blown flap STOL aircraft could cause similar or even higher induced incidence angles (ref. 9).

Fan rotor blade angle. - A test of the fan in a compressor test facility (ref. 1) revealed that design weight flow and pressure ratio could not be attained at design rotational speed for the design rotor blade angle. Tests at both higher and lower blade angles did not reveal any significant improvement in the overall fan performance. Therefore, for other than reverse-thrust tests and a single forward-thrust test at a blade angle 5° lower than the design value, the data reported herein were obtained with the rotor set at the design angle which was discussed in the section Fan stage.

Instrumentation interference. - To evaluate instrumentation interference, measurements were made with the rakes in zones 2 and 4 (fig. 5) removed from the model and also with just the zone 2 rakes removed. The tests were conducted with the bellmouth inlet and with the wind tunnel off. Effects of this instrumentation on fan total pressure ratio, fan weight flow, and model thrust were negligible. All data with tunnel flow were therefore measured with fan inlet and exit rakes installed.

Test sequence. - The normal test variable sequence used in obtaining data with a given configuration was to set the tunnel velocity with the fan windmilling and the model

at zero incidence angle, then to increase the fan rotational speed to the desired level, and, finally, to measure data at successively increasing values of incidence angle. A series of tests to determine the effects of varying this sequence were conducted with a single nacelle configuration: inlet cowl $A_1/A_T = 1.35$, spinner L, and nozzle $A_e/A_3 = 1.11$.

A test to determine repeatability of data using the normal sequence of test variables resulted in no significant variation of pressure and temperature data measured at different times. Force balance data repeatability was within the 3 percent accuracy band defined by the calibration test. Repeatability data were obtained at a tunnel velocity of 44 m/sec (143 ft/sec), fan rotational speeds of 90 and 110 percent of design speed, and model incidence angles from 0° to 50°. A hysteresis test was conducted at the same conditions, but with data measured at decreasing values of incidence angle. No hysteresis effect was discerned.

Two other variations in test sequence were considered. First, the tunnel velocity was held constant at 44 m/sec (143 ft/sec), the model incidence angle was fixed at angles between 0° and 50°, and the fan speed was varied between 90 and 110 percent of the design value. Data obtained at a succession of steady-state conditions indicated no effect of this variation in test sequence.

Next, the model incidence angle was set at 50°, the fan speed was set at 100 percent, and the tunnel velocity was increased from the wind-tunnel-off condition to 44 m/sec (143 ft/sec) and then reduced to the wind-tunnel-off condition. An effect of this variation in test sequence was obtained and is discussed in the section Performance Sensitivity to Test Sequence. Although the difference in results caused by the variation of test variable sequence is of concern, we believe that the normal sequence most closely approximated steady flight conditions, and, therefore, all other data reported herein were obtained with it.

Reverse-Thrust Tests

Fan rotor blade angle. - A series of tests with the wind tunnel off and with various rotor blade angles were conducted to determine the effect of rotor angle on the fan reverse-thrust force. Two methods of achieving reverse thrust were considered. First, the rotor blades were rotated through the feathered angle (clockwise direction in fig. 2) and data were obtained at 75°, 80°, 85°, 90°, 95°, and 100° ($+\Delta\gamma$) from the design condition shown in figure 2. The other type of reverse flow test was obtained by rotating the blade through the flat angle (counterclockwise direction). Data were obtained at 85° and 95° ($-\Delta\gamma$) from the design condition for this case. Blade rotation through the feathered angle results in the conventional blade trailing edge becoming the blade leading edge in reverse pitch, but the correct blade camber is maintained. The

opposite effects are true for blade rotation through the flat angle.

Tunnel velocity and model incidence angle. - Reverse-thrust data were obtained at tunnel velocities ranging from the tunnel-off condition to 43 m/sec (140 ft/sec). Data at model incidence angles other than zero are not presented because of a vibration problem which caused erratic force balance measurements and unsafe operating conditions. The cause of this vibration seemed to be the interaction of the tunnel flow and the reversed fan jet.

Fan speed. - The same values of fan equivalent speed as in the forward-thrust tests were used in the reverse-thrust tests with the wind tunnel off to determine the effect of rotor blade angle on reverse thrust. Only data measured at fan speeds equivalent to 90 and 110 percent of design are reported. During the test with tunnel flow, no data were obtained at the design speed because of unsafe vibration of the model, a condition which was unique to the model.

Data Reduction and Presentation

Explanations of some data reduction procedures are given in the following sections. The discussion relates only to the forward-thrust tests, except for the section on thrust measurements, which relates to both forward- and reverse-thrust tests.

Inlet pressure recovery. - Area-averaged values of inlet pressure recovery (i.e., the ratio of average fan face total pressure to wind tunnel total pressure) were calculated by using data from all the pitot tubes at the fan face location (zone 2, fig. 5). Total pressures at the circumferential locations of the flow rakes and the radial positions of the boundary layer rakes were determined by linear interpolation. Areas were associated with these interpolated values of total pressure and with the data from the boundary layer rakes by equally dividing the radial and circumferential distances between adjacent tubes or points where interpolations were made.

Inlet flow distortion. - Two inlet flow distortion parameters are presented. The first distortion parameter is defined as the difference between the maximum and minimum values of total pressure at the fan face divided by the area-averaged value of total pressure.

$$DI_{max} = \frac{P_{t2,max} - P_{t2,min}}{P_{t2,av}} \tag{1}$$

The area-averaged total pressure was determined by using data from all pitot tubes of the flow rakes and boundary layer rakes. In determination of the maximum and minimum values of total pressure, only those pitot tubes which were not inside the boundary layer

at 0° model incidence angle were used. On the hub side of the fan duct, the closest pitot tube to a surface which was used in defining maximum and minimum total pressures was separated from the surface by 8 percent of the duct cross-sectional area. On the tip side of the fan duct, the closest pitot tube used was separated from the surface by 8 percent of the duct cross-sectional area for the short cowl (inlet cowl $A_1/A_T = 1.26$, fig. 3) and by 15 percent of the duct cross-sectional area for the long cowl (inlet cowl $A_1/A_T = 1.35$, fig. 3).

The second distortion parameter is defined as the difference between the area-averaged fan face total pressure and the minimum value of total pressure averaged over any 60° sector of the fan face divided by the area-averaged fan face total pressure.

$$DI_{60} = \frac{P_{t2,av} - P_{t2,min60}}{P_{t2,av}} \tag{2}$$

All pitot tubes in both flow and boundary layer rakes were used to define the required average pressures. This parameter is particularly useful as a measure of circumferential distortion.

Fan weight flow measurement. - A common problem in wind tunnel tests of aircraft engines or engine models is weight flow measurement. In the present experiment, a theoretical potential flow calculation (ref. 10) was used. The measured ratio of static to total pressure at the outer side of the annular duct at the fan face (zone 2, fig. 5) was applied to a weight flow calibration predicted by theoretical potential flow. A single variation of inlet static- to total-pressure ratio with weight flow for the theoretical potential flow was obtained for each cowl. This variation was taken to be the same for all model incidence angles. The calibration was applied to the measured ratio of static to total pressure on the outer surface in each of six sectors, evenly spaced around the duct circumference; and the total weight flow was obtained by a summation of weight flows from each sector. Each sector had a flow rake at its center, and average values of the sector total pressure and cowl surface static pressure were determined from the measurements within the sector.

Comparison of the weight flow determined by this method with that determined directly with the bellmouth inlet indicated a difference of about 2 percent. An approximate boundary layer calculation indicated that most of this difference could be attributed to boundary layer growth at the fan inlet. No boundary layer corrections were made to the data presented herein, and they are considered generally accurate to within 2 percent. The weight flow measurement is considered to have been less accurate when the inlet flow was highly distorted. For cases where the bellmouth inlet was used, the weight flows determined with it are presented, and these are considered accurate to about 1 percent.

Fan total pressure ratio. - For the purpose of calculating the fan stage total pressure ratio, a mass-averaged value of the stage inlet total pressure was determined by using average static pressures in each of the six sectors discussed in connection with weight flow measurement. These were combined with the total pressures measured with the flow rakes to determine the weight flows necessary for mass averaging.

The stage outlet total pressure was measured with the rakes at the fan stage exit (zone 4, fig. 5). To account for the stator wakes, adjustments were made based on the data obtained in the compressor test facility (ref. 1) with similar fixed rakes and with traversing-type instrumentation which directly measured the effects of stator wakes. It was determined that the difference in stage total pressure ratio measured with these two techniques was generally less than 0.005. A correction factor based on a linear relation between the fixed rake and traversing probe data, and independent of fan speed, was found adequate to correct the fixed-rake data determined with the engine model instrumentation. The pressure ratio so corrected was a mass-averaged value obtained by assuming a linear variation in static pressure between the hub and tip values. Although the fan stage total pressure ratio data reported herein were determined by mass averaging, area-averaged values were also calculated. Significant differences between the two methods of analysis occurred only when the inlet flow was highly distorted.

Fan thrust. - The thrust data reported herein were obtained from the force balance measurement along the model axis with the drive turbine thrust subtracted. Drive turbine thrust was calculated from the measured turbine weight flows, and an ideal discharge velocity based on turbine exit total pressure and temperature and the tunnel static pressure.

FORWARD-THRUST RESULTS

Fan Stage Performance

Results of tests with the wind tunnel off and with the bellmouth inlet used to determine the effect of fan nozzle area on fan performance are presented in figure 8. These results are shown with the fan map (total pressure ratio against weight flow) determined in the compressor test facility (ref. 1). It was determined in the compressor facility tests that the blade stresses were at a safe level when the fan was operated at weight flows slightly lower than those corresponding to the stall line shown in figure 8. Therefore, the stall margins with all three nozzles were considered adequate. The nozzle with the area ratio A_e/A_3 of 1.11 was selected for most of the wind tunnel tests because it approximated the maximum efficiency points for the fan performance (ref. 1). A single tunnel flow test was conducted with the nozzle having an area ratio A_e/A_3 of 1.03.

Inlet Performance

The data presented in this section were measured at a tunnel velocity of about 44 m/sec (143 ft/sec) with a fan nozzle area ratio A_e/A_3 of 1.11. Only fan speeds equivalent to 90 and 120 percent of the design speed are discussed. The inlet design variables considered are inlet cowl contraction ratio and spinner length.

Pressure recovery. - An effect of inlet cowl contraction ratio A_1/A_T on inlet performance is shown in figure 9 where inlet total pressure recovery is presented as a function of model incidence angle. The inlet configurations considered had contraction ratios A_1/A_T equal to 1.26 and 1.35 and spinners which projected to the throat of each cowl. Data for the low-contraction-ratio case show that large reductions in pressure recovery occurred at incidence angles greater than 30^o for both fan speeds. Data for the high-contraction-ratio case show that a similar large reduction in pressure recovery occurred at 90 percent fan speed; but, at 120 percent speed, the pressure recovery remained at a high level through the entire range of incidence angles. Other data will be presented to indicate that the large, sudden reductions in pressure recovery were related to separation of the cowl internal flow.

Two other points concerned with the inlet performance should be noted. First, the case where pressure recovery remained high over the entire range of angles had a throat (minimum inlet duct cross-sectional area) Mach number of 0.73, which was the highest value attained in this experiment. Finally, at low angles with attached flow, figure 9 shows that the inlet with the lower contraction ratio had slightly higher values of pressure recovery. This inlet was shorter and had a lower throat Mach number than the high-contraction-ratio configuration, and, therefore, duct losses were smaller. As an example, at 120 percent speed, where the throat Mach number for the high-contraction-ratio inlet was 0.73, the comparable Mach number for the low-contraction-ratio inlet was 0.66.

The effect of spinner length on inlet performance is indicated in figure 10. Average inlet pressure recovery is shown as a function of incidence angle for the inlet cowl with an A_1/A_T of 1.35 and for two spinners described in figure 3, which vary in length. A small advantage is shown for the long spinner, especially at 90 percent fan speed, where the decrease in pressure recovery because of flow separation occurred at a higher incidence angle than for the short spinner.

Total pressure contours. - A series of fan face total pressure contours progressing to the highest measured distortion and lowest pressure recovery are shown in figure 11. The case considered is the low-contraction-ratio configuration previously considered at 120 percent fan speed. Progression is from low to high incidence angle, and the average pressure recovery is given with each contour. The outer line of the contour represents the fan tip, and the inner line represents the fan hub. The bottom of each contour corresponds to the windward side or leading edge of the inlet as incidence angle increases.

Boundary layer separation on the windward side is indicated between 30° and 40° by the large increase in the area of low local total pressure recovery shown by comparing the contours in figure 11(c) with those of figure 11(b).

Flow distortion. - Figures 12 and 13 show how two inlet flow distortion parameters vary with model incidence angle for the cases previously considered in figure 9. Large increases in distortion occurred at incidence angles greater than 30° for the same cases that exhibited low pressure recovery in figure 9. The high-contraction-ratio and high-fan-speed case again showed relatively good performance.

Static pressure distribution. - Distributions of the ratio of surface static pressure to wind tunnel total pressure along the windward side of the inlet duct are shown in figure 14 for the cases considered in figures 9, 12, and 13. Data measured at 90 percent fan speed are given in figure 14(a) at incidence angles prior to boundary layer separation and following separation for the two inlets, with the separation cases so labeled. Inlet lip separation occurred for both inlets at this fan speed, and this is made evident by the relatively flat pressure distributions downstream of the point of separation, near the leading edge or highlight. The throats of both inlet cowls are at about an X/X_{max} of 0.2 (fig. 3). The observation that separation occurred for the high-contraction-ratio inlet case at 50° (fig. 14(a)) is not as clear as for the low-contraction-ratio case, but a comparison of the static pressures at 50° with those at 40° shows an increase on the inlet lip ($X/X_{max} < 0.2$) with angle and a recovery to a lower value near the fan face. These results and the reduced average total pressure recovery confirm that separation occurred.

The data for 120 percent fan speed are shown in figure 14(b). Separation is again indicated for the low-contraction-ratio inlet. However, as previously observed with the total pressure recovery data, no separation is indicated by the static pressure distribution for the high-contraction-ratio inlet at 50° incidence angle. The data for 40° incidence angle show a possible separation "bubble" near the highlight, but the good recovery indicates that reattachment of the boundary layer resulted. A separation bubble is also indicated at 30° incidence angle for the low-contraction-ratio inlet in figure 14(b). In all cases where separation (i.e., poor recovery) did not occur, high surface Mach numbers were measured. The high-contraction-ratio inlet data of figure 14(b) indicate that Mach numbers of about 2.1 were achieved near the highlight at 50° incidence angle.

Effect of Inlet Variation on Model Thrust Performance

Figure 15 compares the net axial thrust of the model for two inlet configurations over a range of incidence angles. The nacelle configurations and fan speeds are the same as those considered in figures 9 and 11 to 14. Thrust losses at incidence angles greater than 30° occurred for all but the high-contraction-ratio ($A_1/A_T = 1.35$) case at

120 percent fan speed. At 120 percent fan speed and 50° model incidence angle, the low-contraction-ratio ($A_1/A_T = 1.26$) configuration produced a thrust about 17 percent lower than that of the high-contraction-ratio configuration. These results correlate with the inlet performance previously discussed. The increase in thrust with increasing angle shown in figure 15 prior to inlet separation occurs because of a decrease in inlet momentum along the model axis, which is the measurement axis. At angles less than 30°, the low-contraction-ratio inlet configuration produced higher thrust than the high-contraction-ratio inlet configuration, which also correlates with inlet performance. The slightly higher total pressure recovery of the low-contraction-ratio inlet, at low angles, and also its probable lower external drag because of its shorter length contribute to higher values of net thrust.

Fan performance data for the two inlet configurations are given in figures 16 and 17. Figure 16 shows fan weight flow variation with incidence angle. Trends of the weight flow data are consistent with the thrust measurements shown in figure 15. Only the high-contraction-ratio configuration at 120 percent fan speed indicated no weight flow reduction at high angles. The variation in fan stage total pressure ratio with incidence angle is shown in figure 17 for 70, 90, 110, and 120 percent fan speeds. Only the 110- and 120-percent-fan-speed data for the high-contraction-ratio inlet do not indicate reductions in fan pressure ratio for incidence angles greater than 30°. The combination of reduced inlet pressure recovery, reduced stage pressure ratio, and reduced weight flow contributes to the large reductions in thrust at high incidence angles observed in figure 15.

Effect of Nozzle Variation on Model Performance

Figures 18 and 19 show results of an 8 percent variation in fan nozzle exit area. These data indicate that the model performed slightly better with the smaller nozzle at high incidence angles for 120 percent fan speed. The coupled performance of the fan and nacelle with the smaller nozzle allowed a few degrees higher incidence angle than with the larger nozzle before inlet separation caused a reduction in inlet pressure recovery (fig. 18) and net thrust (fig. 19). At low incidence angles, before separation occurred, the nozzle variation had little effect on the net thrust or inlet pressure recovery at either 90 or 120 percent fan speed.

Acoustic Performance

Reverberant sound pressure level spectra resulting from one-third octave frequency band analysis are shown in figure 20 for the two inlet configurations previously dis-

cussed at 120 percent fan speed and with the wind tunnel off. The blade passing frequency (BPF) and a multiple (2 BPF) are noted on the figure. At these conditions, the spectra for the two configurations were very similar, with differences of only about 1 decibel near the blade passing frequency, which was dominant.

Results of acoustic measurements at a tunnel velocity of 44 m/sec (143 ft/sec) are given in figures 21 and 22 for the two inlet configurations. The peak noise levels near the blade passing frequency for 0° incidence angle were 1 to 4 decibels lower than without tunnel flow (fig. 20). This may be an indication of measurement accuracy or a noise convection effect. A background noise spectrum (i.e., with the fan windmilling) is shown in both figures. The background noise was substantially below the spectra obtained with model operation, except at frequencies below about 300 hertz, where the noise levels were about equal.

For the high-contraction-ratio inlet configuration (fig. 21), the shape of the spectrum at 50° was similar to that at 0°, with the biggest difference occurring at high frequencies. At twice the blade passing frequency the sound pressure level increased 5 decibels between 0° and 50°, and at 15 000 hertz the increase was about 9 decibels. Only the increase at the harmonic of the blade passing frequency would be expected to significantly affect the overall sound pressure level because of the sharp drop in level with increasing frequency, assuming no attenuation at these frequencies due to the wind tunnel environment. These increases in noise level, as well as the smaller increases across a broad band of lower frequencies, were most probably caused by a small increase in inlet flow distortion with increasing incidence angle (figs. 12 and 13).

Data for the low-contraction-ratio case (fig. 22) show small increases in noise level over the entire spectrum between 0° and 30° incidence angle, with about a 2-decibel increase at the blade passing frequency and its multiple. Between 30° and 40°, a large increase in noise level occurred over a broad band of frequencies. At the blade passing frequency, the increase was about 5 decibels and was as high as 14 decibels over a broad band below the blade passing frequency. This broad-band increase would affect the overall sound pressure level because of its extent and its level being near the peak at 30°. The dramatic change in the noise spectra between 30° and 40° correlates with the inlet flow separation previously discussed for this configuration. The changes in the noise spectra between 40° and 50° were modest and associated with small increases in inlet flow distortion. For 50°, the low-contraction-ratio case had a sound pressure level about 9 decibels higher than that of the high-contraction-ratio case near the blade passing frequency.

Performance Sensitivity to Test Sequence

As mentioned in the section Test sequence, a sensitivity of model performance to

test variable sequence was observed. With the model angle fixed at 50° and the fan speed at 100 percent, data were obtained at a succession of increasing and decreasing tunnel velocities. Fan thrust data are shown in figure 23, and pressure recovery data are shown in figure 24. These data are compared, in each figure, to data obtained with the normal test sequence, where the model angle was increased from 0° to 50° in a stepwise manner with the tunnel velocity and fan speed fixed. At the highest tunnel velocity, about 44 m/sec (143 ft/sec), the performance obtained with the normal sequence was significantly better than the performance obtained with the successive variation of tunnel velocity. No significant effect of the direction of the tunnel velocity variation was discerned from the small amount of data obtained.

The pressure recovery data (fig. 24) suggest the differences in performance measured at a single operating condition were caused by the sensitivity of inlet boundary layer flow separation to how the operating condition was approached. As stated previously, it is believed that the normal test sequence most closely represented steady flight conditions.

REVERSE-THRUST RESULTS

Effect of Rotor Blade Angle

Data showing thrust variation with rotor blade angle are given in figure 25 at 90 and 110 percent fan speeds. These data were obtained with the bellmouth nozzle (fig. 4(b)) and the wind tunnel off. Reverse-pitch data are compared with forward-thrust data (i.e., fan with conventional pitch, at the design blade angle (0°) and at an incidence angle 5° lower than the design angle. The reverse-thrust levels attained with blade rotation through the feathered angle were about 1.8 times those with blade rotation through the flat angle. No optimum rotor angle for reverse thrust could be determined with the small range of angles examined. Because of the lack of actual static conditions, it is difficult to compare the reverse- and forward-thrust levels. Drag forces, including inlet momentum, and incorrect fan backpressures caused by the induced tunnel flow might result in thrust values somewhat different from what would have occurred for actual static conditions. However, actual measures of these effects cannot be obtained from the available data. A direct comparison of the largest measured values of reverse thrust to the forward thrust at the design rotor angle shows that the greatest reverse thrust attained (with rotation through feather) was equal to about 60 percent of the forward thrust at each of the fan speeds.

Effect of Tunnel Velocity

Reverse-thrust variation with tunnel velocity, for a blade angle 100^{o} from the design setting obtained by rotation through the feathered angle is shown in figure 26 for 90 and 110 percent fan speeds. Comparable forward-thrust data are shown in the same figure. Over the range of tunnel velocities considered, an increase in tunnel velocity resulted in a reduction of reverse thrust. The reduction was about 30 percent at 90 percent fan speed and 50 percent at 110 percent fan speed. Two possible reasons for the reduction in reverse thrust with increasing tunnel velocity were a reduction in reverse flow inlet pressure recovery and a reduction in fan weight flow caused by the interaction of the tunnel flow and the reversed fan jet. Recall that the reverse-thrust inlet was the fan aft duct for the forward-thrust case. At the lowest velocity indicated in figure 26, where the wind tunnel was off and flow was induced by the model, the reverse thrust forces were about the same as those previously indicated in figure 25. This indicates that the flared nozzle, used with tunnel flow, performed similarly to the bellmouth nozzle (fig. 4(b)).

Comparison of forward- and reverse-thrust data in figure 26 shows that the thrust lapse curves have similar slopes or gradients. At the highest tunnel velocity, which approximated a typical STOL aircraft landing speed, the reverse-thrust force was about 40 percent of the forward-thrust force at 90 percent fan speed and about 35 percent of the forward-thrust force at 110 percent fan speed.

Noise performance for reverse-thrust conditions is given in figure 27 for the same rotor angle and fan speeds considered in the previous figure. An increase in noise level over a broad band of frequencies occurred for both fan speeds between the near static condition and the typical landing velocity. At 90 percent fan speed, the increase was about 3 decibels at the blade passing frequency and somewhat greater at both higher and lower frequencies. At 110 percent fan speed, the increase was about 7 decibels at the blade passing frequency and, again, somewhat greater at other frequencies. The increase in noise level over a broad band of frequencies was attributed to reverse flow inlet performance and to interaction between the tunnel flow and the reverse fan jet. Assuming no frequency selective attenuation, the broad-band increase in sound pressure level could cause a significant increase in overall sound pressure level.

A comparison of the reverse-thrust noise data at 110 percent fan speed presented in figure 27(b) with forward-thrust noise data given previously for 120 percent fan speed (fig. 22) indicates that reverse-thrust noise levels may be higher because of high sound pressure levels over a broad frequency range. At the typical STOL aircraft landing velocity and 0^{o} model incidence angle, noise levels at the blade passing frequencies were approximately equal. But at both higher and lower frequencies, the spectrum for reverse thrust (fig. 27(b)) was as much as 10 decibels higher than that for forward thrust (fig. 22). Poor flow through the fan stage blade rows would probably cause higher noise

for a fan in reverse pitch than for the same fan, operating under comparable conditions, in conventional pitch.

SUMMARY OF RESULTS

A fan engine model with a 50.8-centimeter (20-in.) diameter, 1.15-pressure-ratio fan with a variable-pitch rotor was tested in an isolated nacelle configuration at wind tunnel velocities from 0 to 44 m/sec (143 ft/sec) and at model incidence angles from 0° to 50°. Two inlet cowls having lip-area contraction ratios of 1.26 and 1.35 were tested with two spinners, and two fan nozzles with an 8 percent exit-area difference were also examined in the wind tunnel tests. Tests of reverse-thrust performance with no wind tunnel flow were conducted to determine the effect of rotor blade pitch angle, and a wind tunnel test investigated the effect of forward speed on reverse thrust. Upstream reverberant noise levels were measured for both the forward- and reverse-thrust cases. The following major results were indicated:

1. Higher pressure recovery was measured with an inlet having a lip-area contraction ratio of 1.26 than with an inlet having a contraction ratio of 1.35 at incidence angles below 30°, but above 30° the high-contraction-ratio inlet performed better. For the 1.26-contraction-ratio inlet, internal flow separation on the cowl lip occurred for incidence angles greater than 30° at both 90 and 120 percent fan speeds. For the 1.35-contraction-ratio inlet, separation occurred at 90 percent fan speed but not at 120 percent speed.

2. Inlet flow separation caused decreases in both fan weight flow and stage pressure ratio. It also resulted in thrust for a 1.26-contraction-ratio inlet that was 17 percent lower than that for a 1.35-contraction-ratio inlet, for 120 percent fan speed and 50° model incidence angle.

3. At 50° incidence angle, inlet flow separation also caused the 1.26-contraction-ratio configuration to have a sound pressure level that was 9 decibels higher than that of the 1.35-contraction-ratio configuration near the blade passing frequency. Increased noise level also occurred over a broad band of frequencies below the blade passing frequency.

4. A small advantage in inlet performance was measured at high model incidence angles for an inlet with a spinner that projected to the cowl throat when compared with an inlet having the same cowl but a shorter spinner.

5. A comparison of model performance between two nozzles having an 8 percent exit-area difference showed that the model gave slightly better inlet recovery and thrust performance with the smaller nozzle at high model incidence angles and high fan speed.

6. Model performance was affected by the sequence of test variables. Thrust and inlet pressure recovery were higher when tunnel velocity was set at 44 m/sec

(143 ft/sec), fan speed was set at its design value, and the model angle was increased in a stepwise manner to 50°, than when the fan speed and model angle were set at these values and the tunnel velocity was increased in a stepwise manner to about 44 m/sec (143 ft/sec).

7. Reverse-thrust forces obtained with blade rotation through the feathered blade angle were about 1.8 times larger than with blade rotation through the flat angle.

8. Reverse thrust was reduced from 30 to 50 percent between the wind-tunnel-off condition and a typical STOL aircraft landing velocity.

9. Noise levels associated with reverse thrust at 0° incidence angle increased between 3 and 7 decibels near the blade passing frequency between the wind-tunnel-off condition and a typical STOL aircraft landing velocity. Increased sound pressure level occurred over a broad band of frequencies. Reverse-thrust noise levels may be greater than forward-thrust values at the same fan speed.

Lewis Research Center,
National Aeronautics and Space Administration,
Cleveland, Ohio, February 26, 1974,
501-24.

REFERENCES

1. Osborn, Walter M.; and Steinke, Ronald J.: Performance of a 1.15 Pressure Ratio Axial-Flow Fan Stage with a Blade Tip Solidity of 0.5. NASA TM X-3052, 1974.

2. Wasserbauer, Charles A.: Calculated Performance Map of a $4\frac{1}{2}$-Stage 15.0-Centimeter- (5.9-In.-) Mean-Diameter Turbine Designed for a Turbofan Simulator. NASA TM X-2822, 1973.

3. Baals, Donald D.; Smith, Norman F.; and Wright, John B.: The Development and Application of High-Critical-Speed Nose Inlets. NACA TR-920, 1948.

4. Douglass, W. M.: Aerodynamic Installation of High-Bypass Ratio Fan Engines. Paper 660732, SAE, Oct. 1966.

5. Hancock, J. P.; and Hinson, B. L.: Inlet Development for the L-500. Paper 69-448, AIAA, June 1969.

6. Fasching, Walter A.: Air Force Advanced Lift Fan and Lift/Fan Demonstration Program. R69AEG150-vol. 2; AFAPL-TR-69-7, vol. 2, General Electric Co. (AD-848983L), Feb. 1969. (Available to qualified requesters from DDC; others from Director, Air Force Materiel Command, Attn: MBC, Wright-Patterson AFB, Ohio 45433.)

7. Anon.: ASME Power Test Codes, Supplement on Instruments and Apparatus, Part 5, Chapter 4, ASME, 1959.

8. Yuska, Joseph A.; Diedrich, James H.; and Clough, Nestor: Lewis 9- by 15-Foot V/STOL Wind Tunnel. NASA TM X-2305, 1971.

9. Albers, James A.: Predicted Upwash Angles at Engine Inlets for STOL Aircraft. NASA TM X-2593, 1972.

10. Albers, James A.: Theoretical and Experimental Internal Flow Characteristics of a 13.97-Centimeter-Diameter Inlet at STOL Takeoff and Approach Conditions. NASA TN D-7185, 1973.

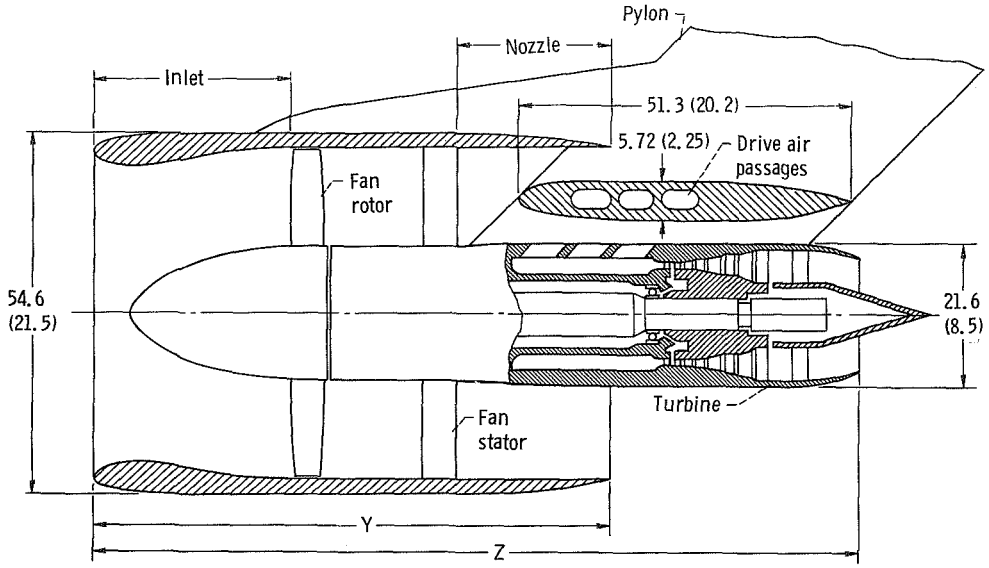

Inlet cowl	Nozzle	Y	Z
1	2	78.7 (31.0)	123.2 (48.5)
1	4 or 5	87.9 (34.6)	123.2 (48.5)
2	4 or 5	95.8 (37.7)	131.1 (51.6)

Figure 1. - Significant fan engine model dimensions. (Dimensions are in cm (in.).)

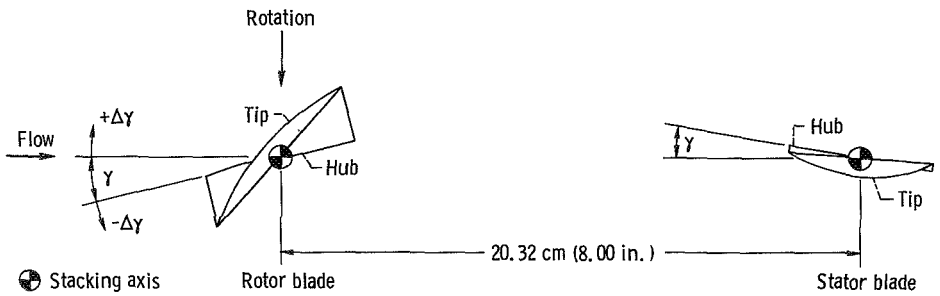

	Rotor blade	Stator blade
Hub chord, cm (in.)	5.27 (2.07)	4.95 (1.95)
Hub setting angle, γ, deg	13.0	9.3
Hub solidity	0.99	2.48
Tip chord, cm (in.)	6.63 (2.61)	4.95 (1.95)
Tip setting angle, γ, deg	48.0	5.1
Tip solidity	0.50	0.99
Blade section	Double circular arc	Double circular arc

Figure 2. - Fan geometry at design condition.

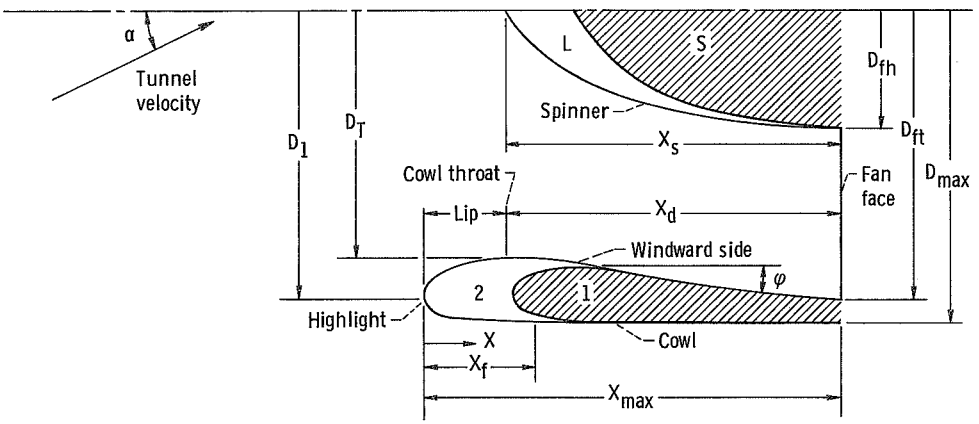

Inlet		Ratio of spinner axial length to maximum diameter, X_s/D_{max}	Inlet cowl contraction ratio, A_1/A_T	Ratio of cowl highlight area to minimum area, A_1/A_{min}	Ratio of inlet duct axial length to maximum diameter, X_d/D_{max}	Ratio of maximum axial length to maximum diameter, X_{max}/D_{max}	Diffuser effective cone angle, deg
Cowl	Spinner						
1	S	0.414	1.26	1.30	0.414	0.516	6.5
2	S	.414	1.35	1.35	.530	.659	4.4
2	L	.530	1.35	1.38	.530	.659	7.8

Figure 3. - Fan inlet geometry and dimensions. Fan tip diameter, D_{ft}, 50.8 cm (20 in.); ratio of fan hub diameter to fan tip diameter, D_{fh}/D_{ft}, 0.4; ratio of maximum diameter to fan tip diameter, D_{max}/D_{ft}, 1.075. External forebody contour: NACA 1-Series; ratio of cowl highlight diameter to maximum diameter, D_1/D_{max}, 0.935; ratio of cowl external forebody axial length to maximum diameter, X_f/D_{max}, 0.175. Lip contour: 2:1 ellipse (long axis parallel to cowl axis). Spinner contour: NACA 1-Series. Diffuser maximum surface angle, φ, 10^0.

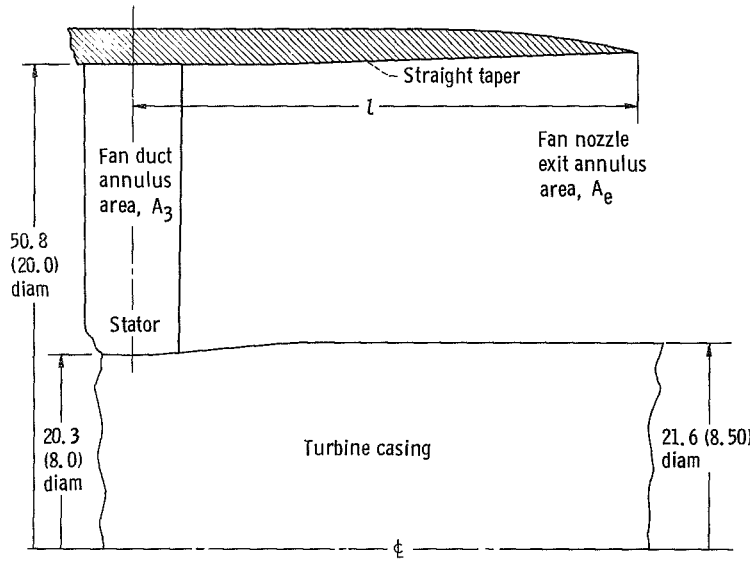

Nozzle	A_e/A_3	Effective cone angle, deg	Nozzle length, l	
			cm	in.
2	1.03	2.0	26.4	10.4
4	1.17	7.3	35.6	14.0
5	1.11	4.5	35.6	14.0

(a) Forward-thrust nozzles. Fan duct annulus area, A_3, 0.170 m^2 (1.833 ft^2) with blade blockage not considered; fan nozzle exit annulus area A_e includes effect of pylon blockage.

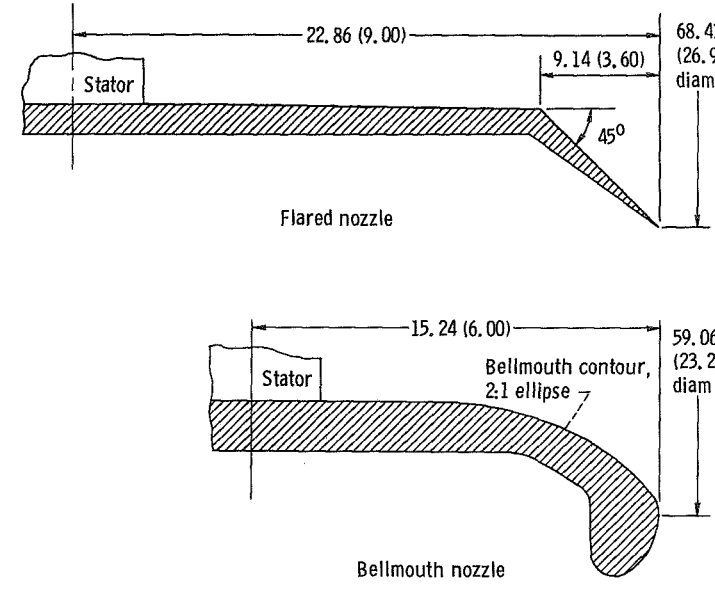

(b) Reverse-thrust nozzles.

Figure 4. - Fan nozzle geometry and dimensions. (Dimensions are in cm (in.).)

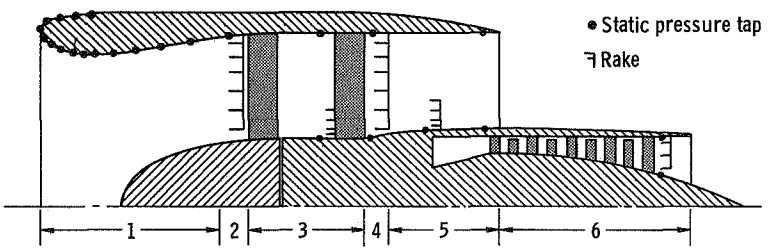

Instrumentation zones

Zone (inlet cowl)	Flow rakes			Boundary layer rakes		Number of static pressure taps	Number of fast-response transducers
	Number of rakes	Number of pitot tubes	Number of thermo-couples	Number of rakes	Number of pitot tubes		
1 (1)						61	
1 (2)						94	
2 (1, 2)	6	36		6	36	12	[a]1
3 (1, 2)				[a]4	[a]16	[a]12	[a]4
4 (1, 2)	6	36	6			12	
5 (1, 2)				[a]4	[a]16	[a]7	[a]3
5 exit (1, 2)						[a]12	
6 (1, 2)	4	6	6			[a]12	

[a]Data from these instruments are not given in this report.

Figure 5. - Model research instrumentation.

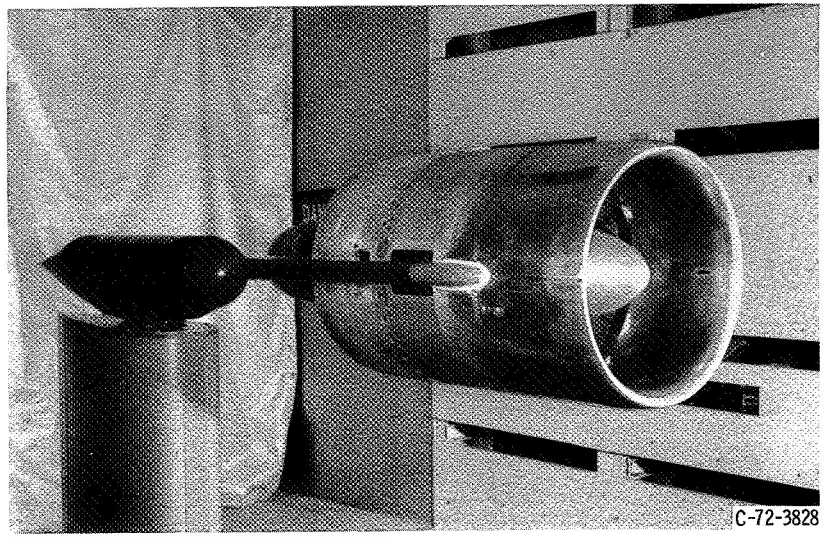

(a) Forward-thrust configuration, front view.

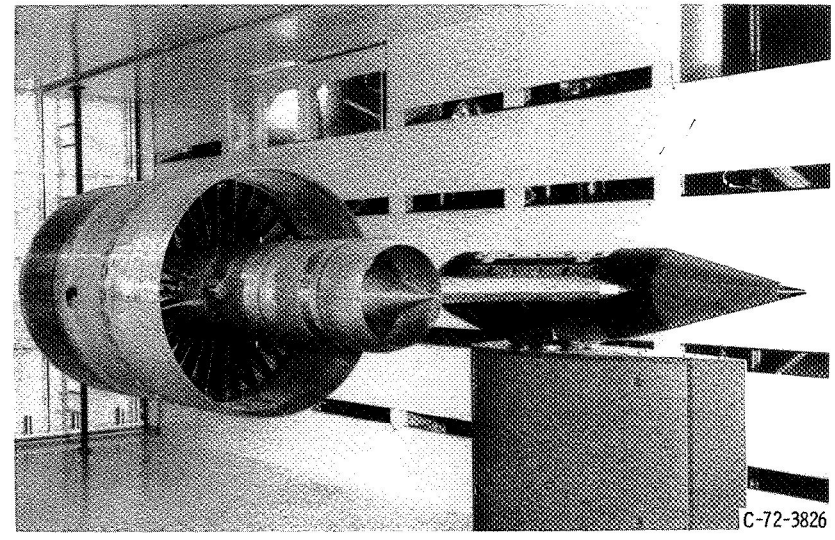

(b) Forward-thrust configuration, rear view.

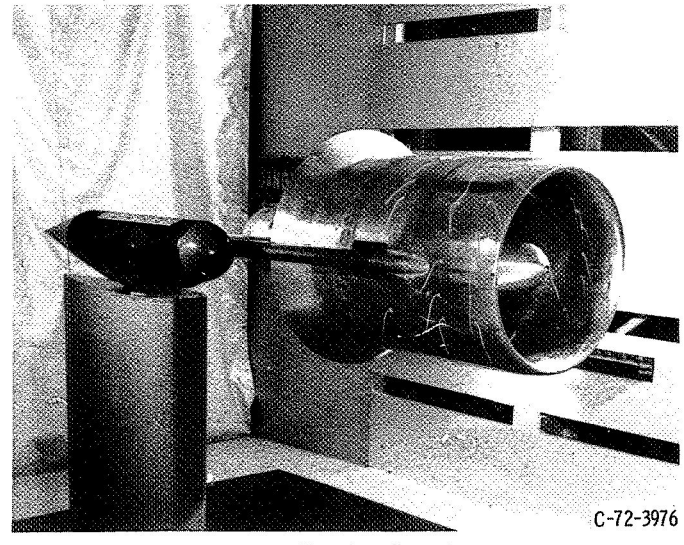

(c) Reverse-thrust configuration.

Figure 6. - Engine model in 9- by 15-Foot V/STOL Wind Tunnel.

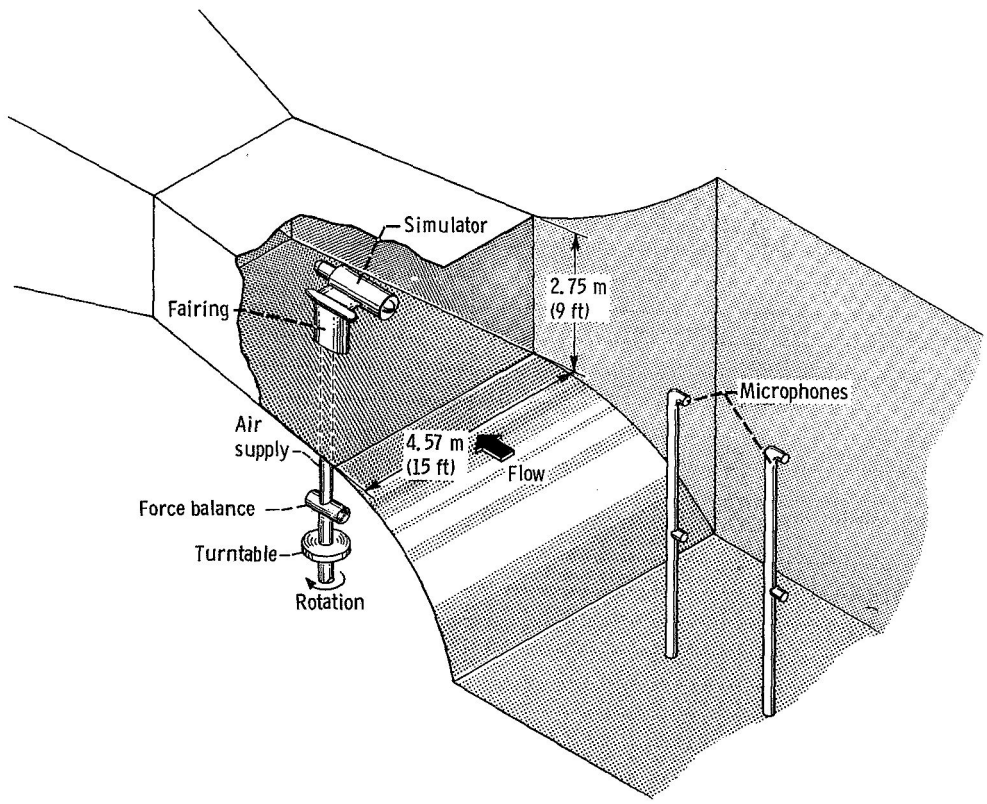

Figure 7. - Model installation in 9- by 15-Foot V/STOL Wind Tunnel.

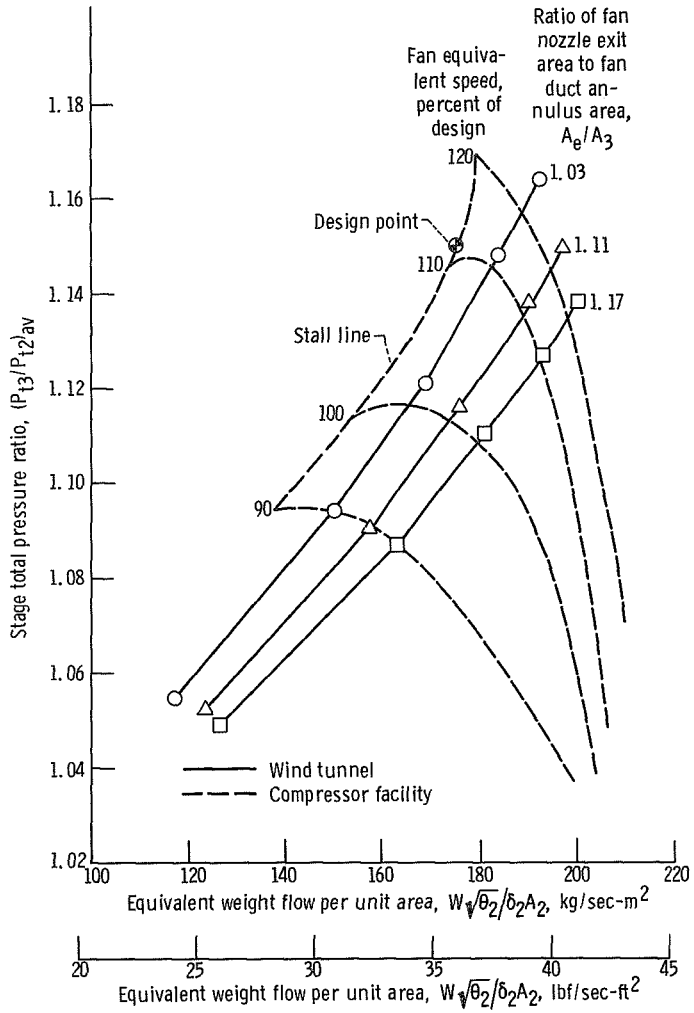

Figure 8. - Fan performance with various nozzles. Fan equivalent design speed, 9160 rpm; wind tunnel off; bellmouth inlet.

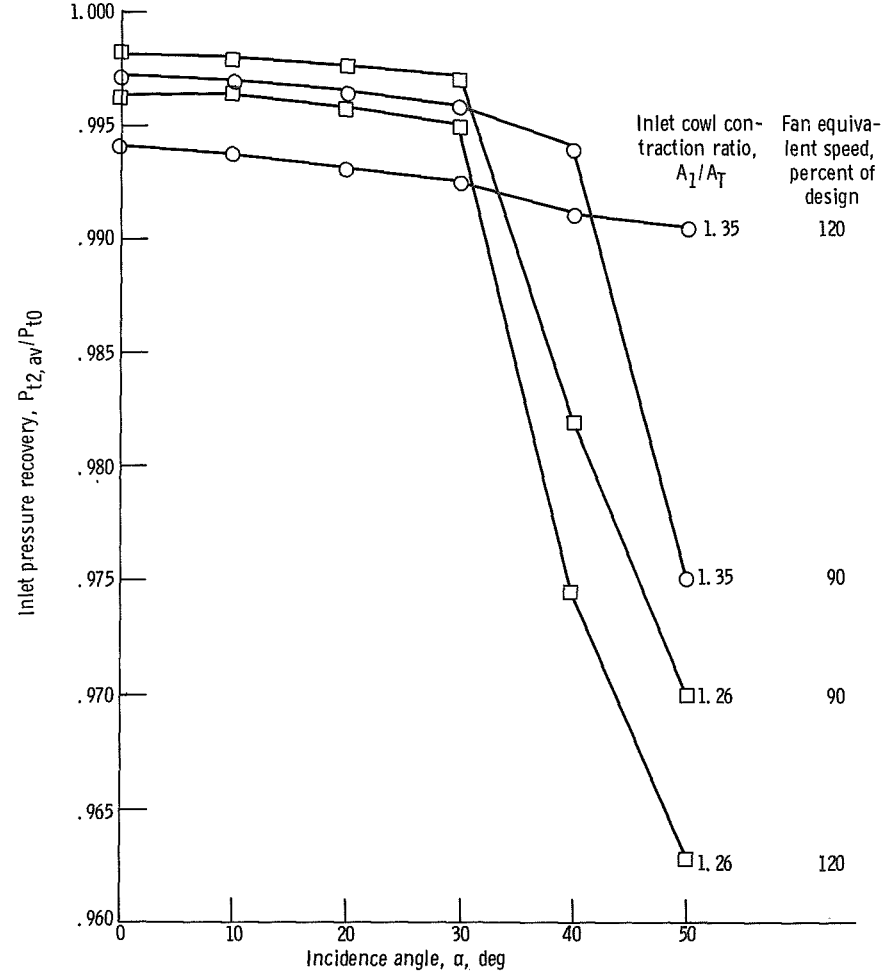

Figure 9. - Total pressure recovery for two inlets. Inlet cowl contraction ratio, A_1/A_T, 1.26 and spinner S; A_1/A_T = 1.35 and spinner L; ratio of fan nozzle exit annulus area to fan duct annulus area, A_e/A_3, 1.11; equivalent tunnel velocity, 44 m/sec (143 ft/sec).

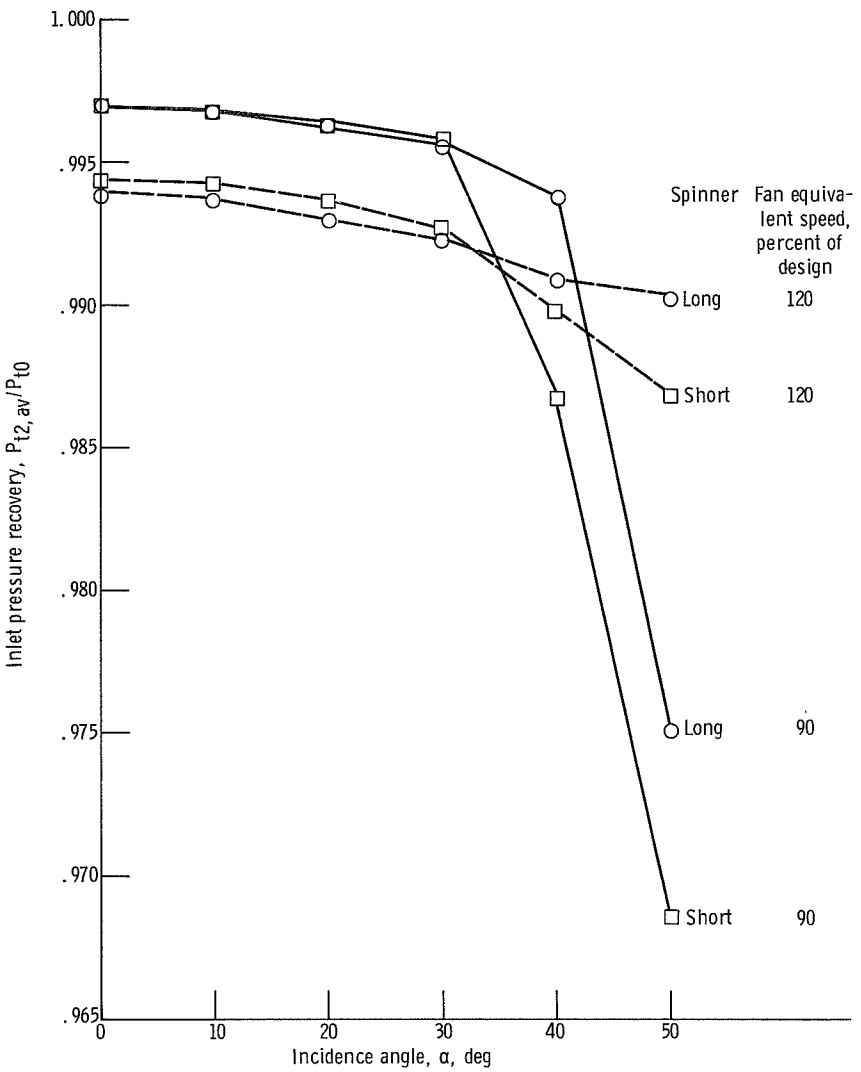

Figure 10. - Effect of spinner length on inlet pressure recovery. Inlet cowl contraction ratio, A_1/A_T, 1.35; ratio of fan nozzle exit annulus area to fan duct annulus area, A_e/A_3, 1.11; equivalent tunnel velocity, 44 m/sec (143 ft/sec).

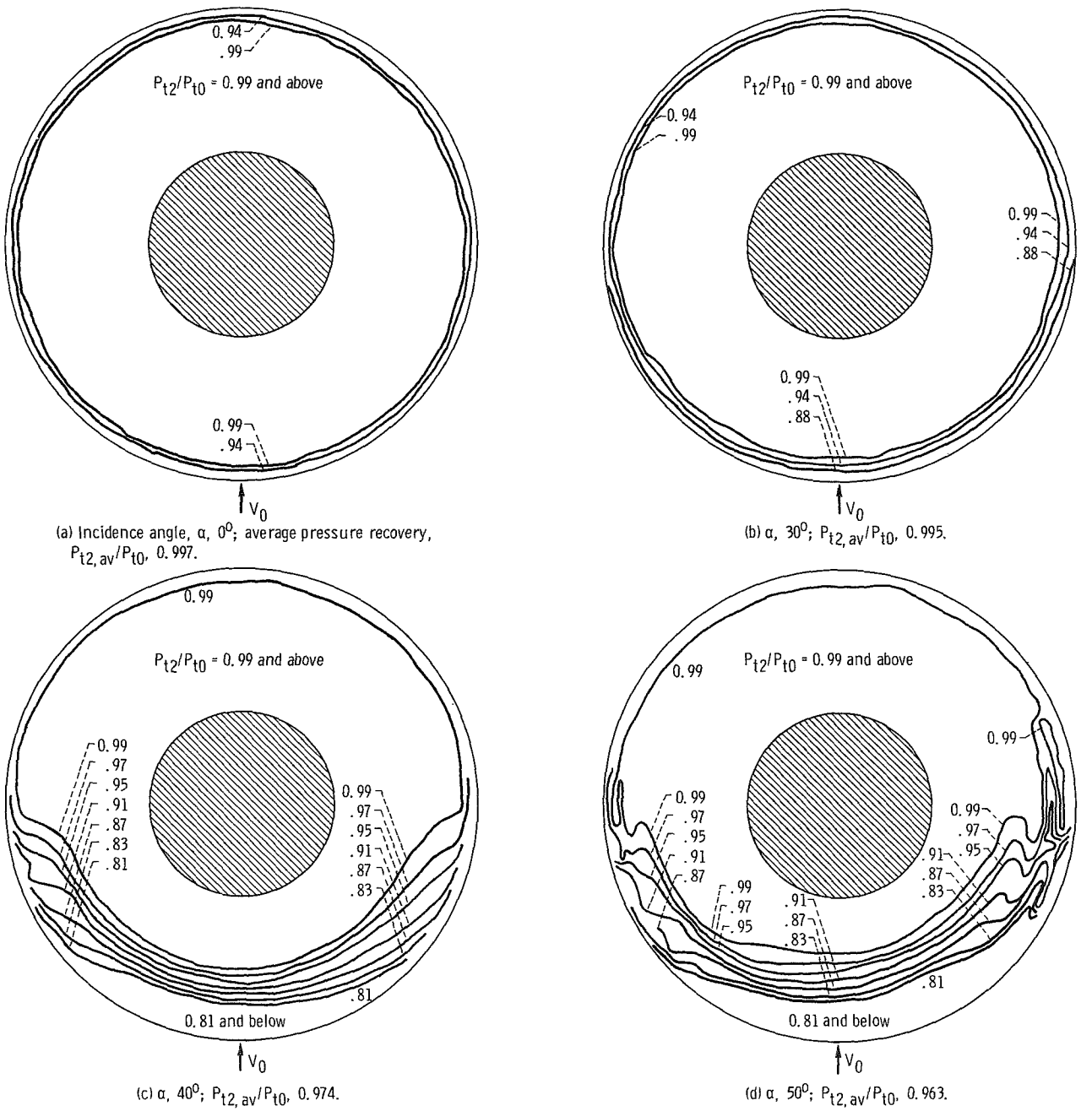

Figure 11. - Fan-face total pressure contours. Inlet cowl contraction ratio, A_1/A_T, 1.26; spinner S; ratio of fan nozzle exit annulus area to fan duct annulus area, A_e/A_3, 1.11; equivalent tunnel velocity, 44 m/sec (143 ft/sec); fan equivalent speed, 120 percent of design.

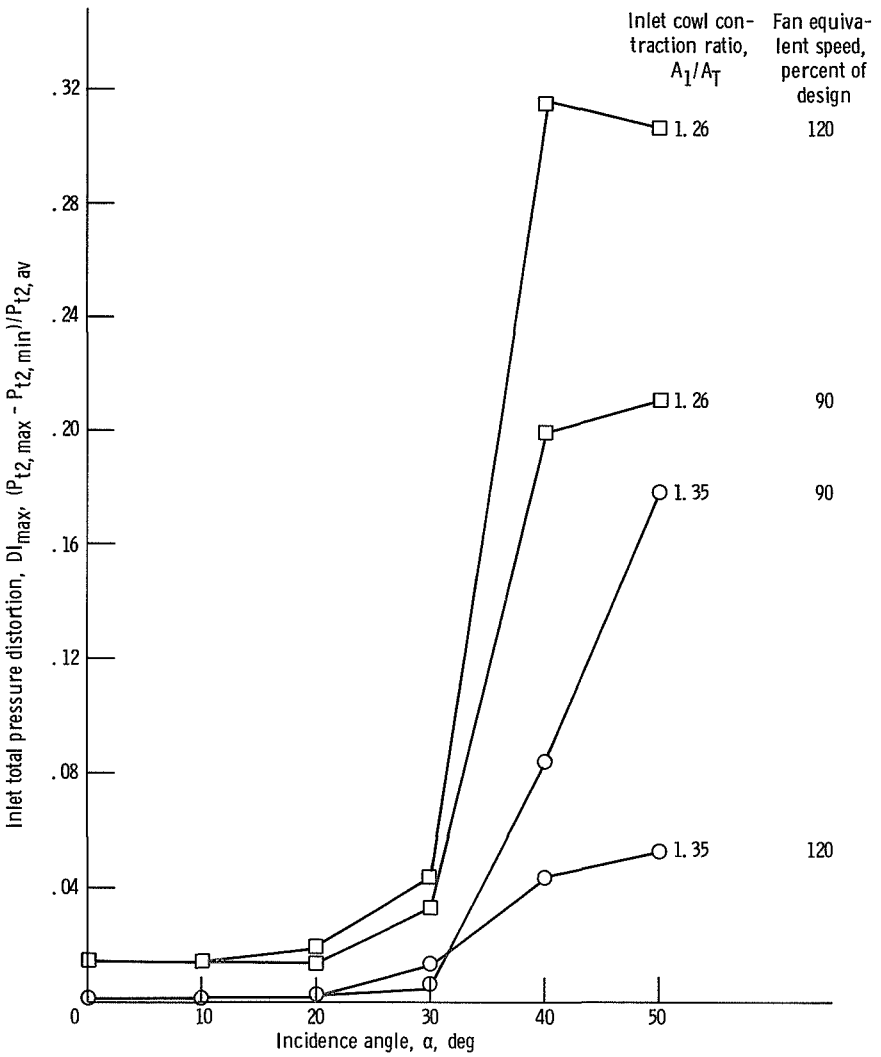

Figure 12. - Total pressure distortion for two inlets. Inlet cowl contraction ratio, A_1/A_T, 1.26 and spinner S; A_1/A_T = 1.35 and spinner L; ratio of fan nozzle exit annulus area to fan duct annulus area, A_e/A_3, 1.11; equivalent tunnel velocity, 44 m/sec (143 ft/sec).

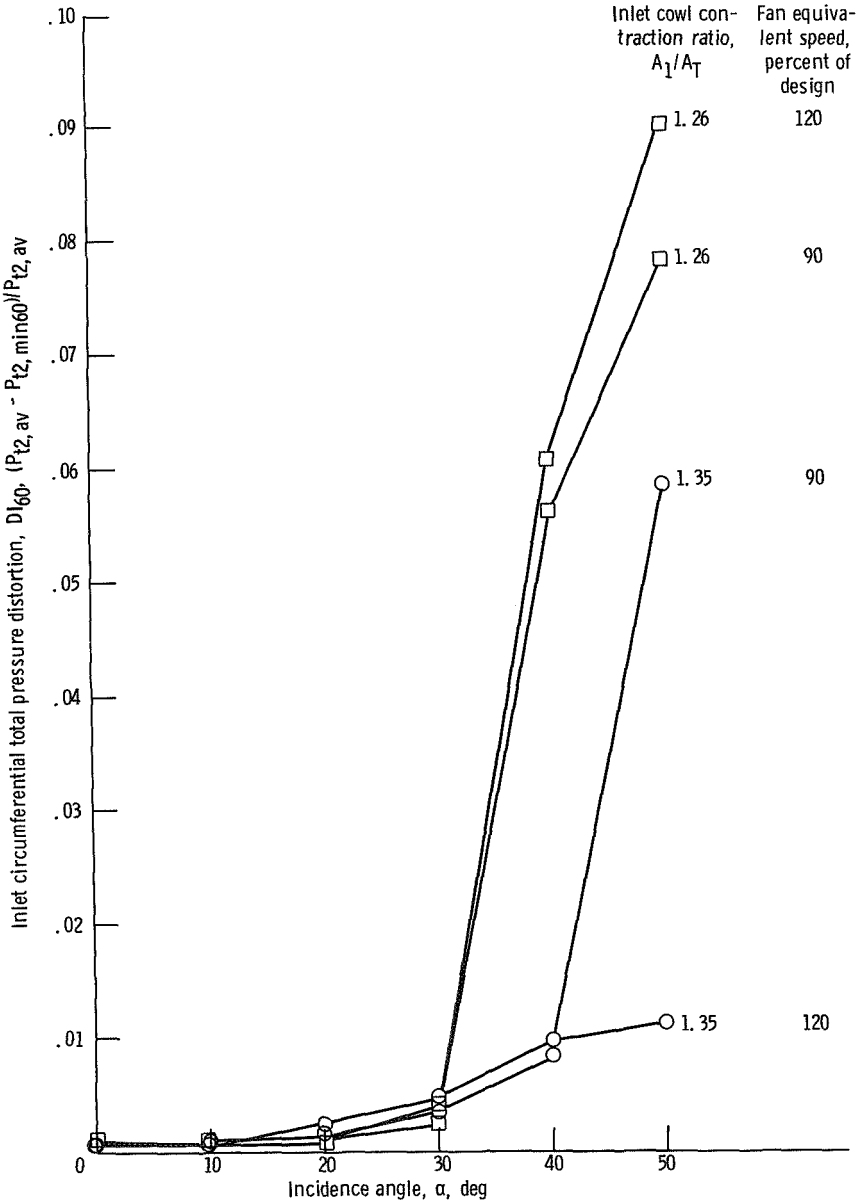

Figure 13. - Circumferential total pressure distortion for two inlets. Inlet cowl contraction ratio, A_1/A_T, 1.26 and spinner S; A_1/A_T = 1.35 and spinner L; ratio of fan nozzle exit annulus area to fan duct annulus area, A_8/A_3, 1.11; equivalent tunnel velocity, 44 m/sec (143 ft/sec).

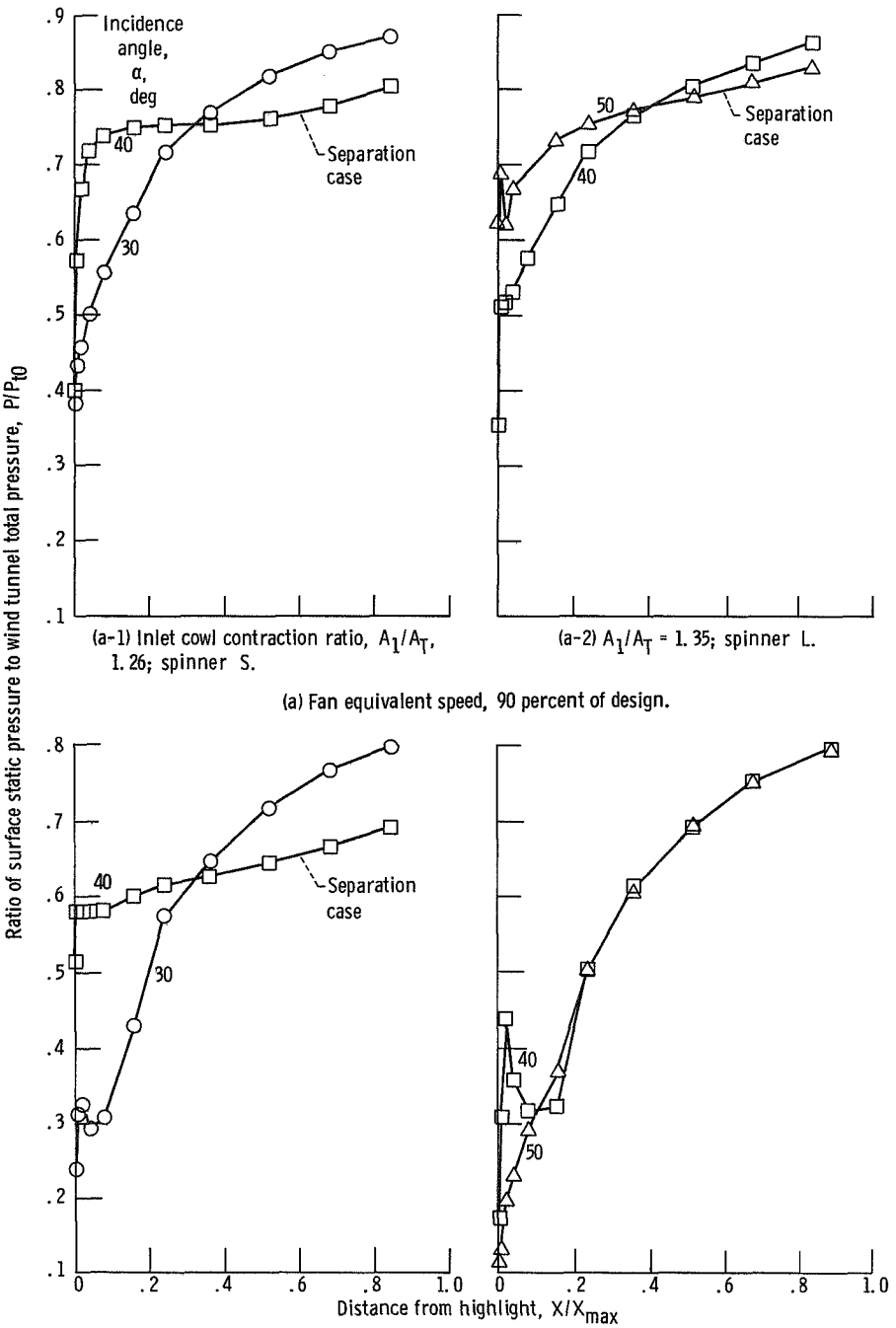

Figure 14. - Inlet duct windward side static pressure for two inlets. Inlet cowl contraction ratio, A_1/A_T, 1.26 and spinner S; A_1/A_T = 1.35 and spinner L; ratio of fan nozzle exit annulus area to fan duct annulus area, A_e/A_3, 1.11; equivalent tunnel velocity, 44 m/sec (143 ft/sec).

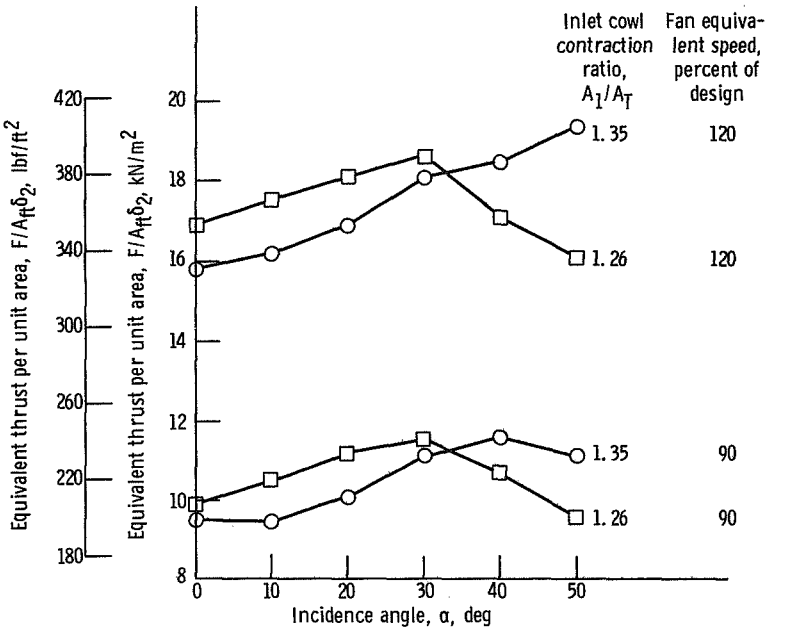

Figure 15. - Model axial thrust for two inlets. Inlet cowl contraction ratio, A_1/A_T, 1.26 and spinner S; A_1/A_T = 1.35 and spinner L; ratio of fan nozzle exit annulus area to fan duct annulus area, A_e/A_3, 1.11; equivalent tunnel velocity, 44 m/sec (143 ft/sec).

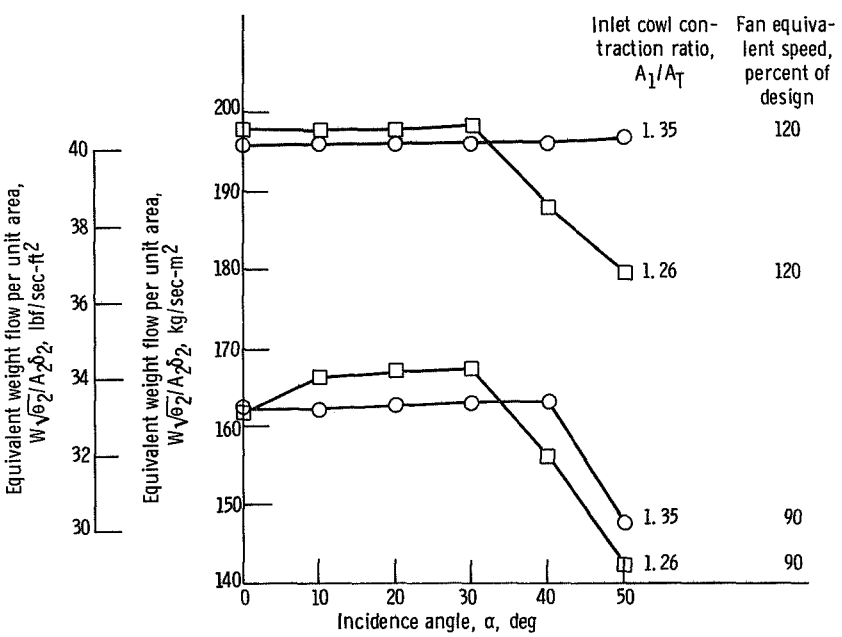

Figure 16. - Fan weight flow for two inlets. Inlet cowl contraction ratio, A_1/A_T, 1.26 and spinner S; A_1/A_T = 1.35 and spinner L; ratio of fan nozzle exit annulus area to fan duct annulus area, A_e/A_3, 1.11; equivalent tunnel velocity, 44 m/sec (143 ft/sec).

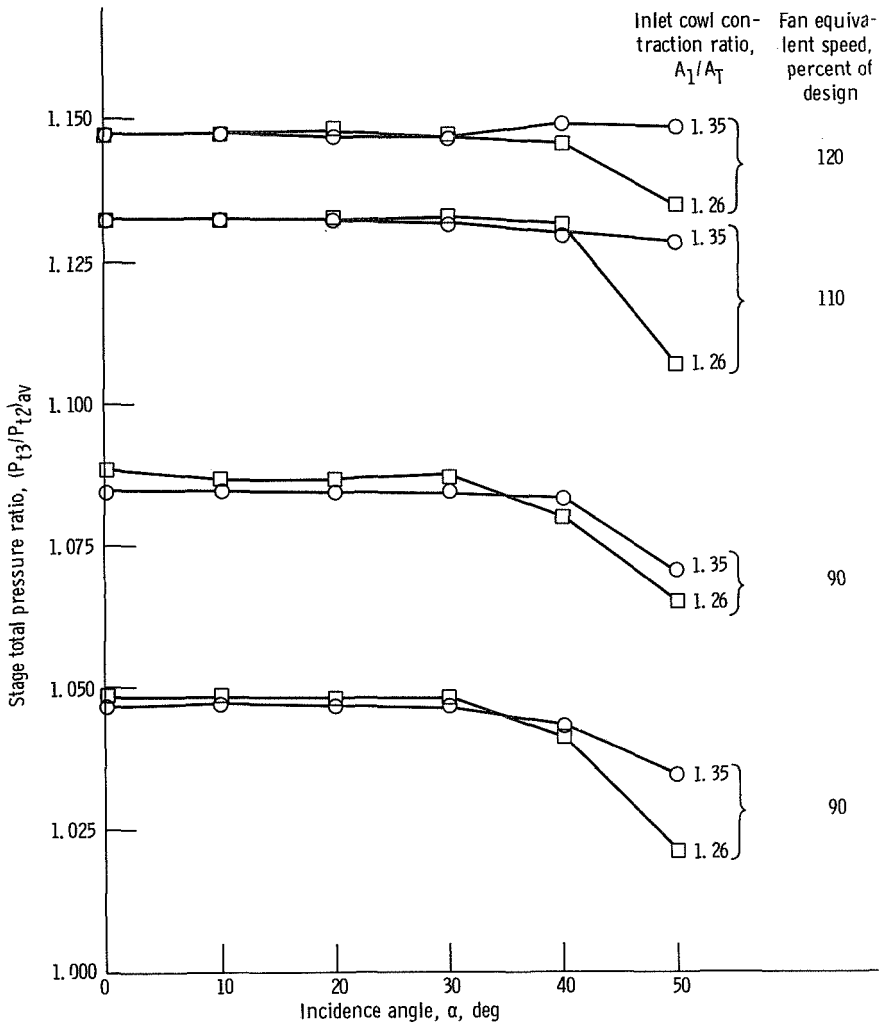

Figure 17. - Fan stage total pressure ratio for two inlets. Inlet cowl contraction ratio, A_1/A_T, 1.26 and spinner S; A_1/A_T = 1.35 and spinner L; ratio of fan nozzle exit annulus area to fan duct annulus area, A_e/A_3, 1.11; equivalent tunnel velocity, 44 m/sec (143 ft/sec).

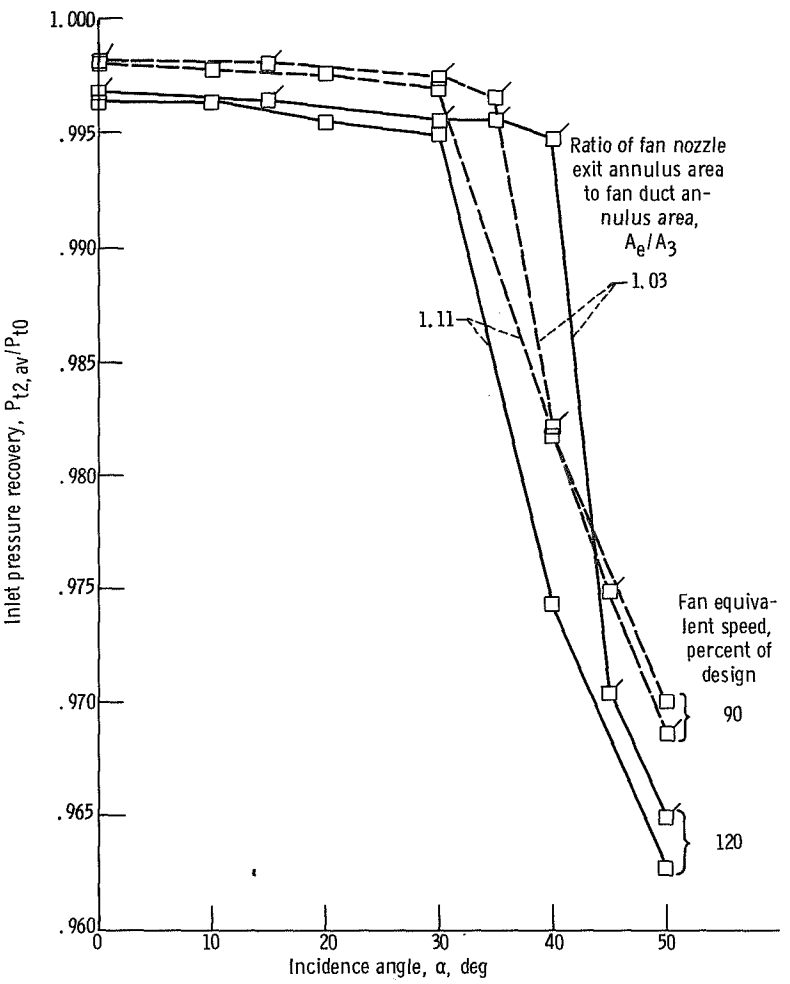

Figure 18. - Inlet total pressure recovery for two nozzles. Inlet cowl contraction ratio, A_I/A_T, 1.26; spinner S; equivalent tunnel velocity, 44 m/sec (143 ft/sec).

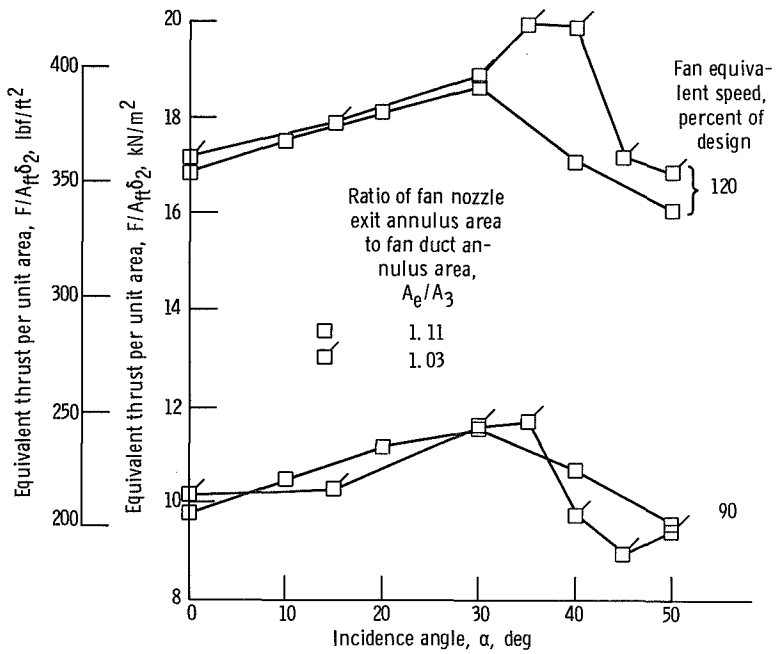

Figure 19. - Model axial thrust for two nozzles. Inlet cowl contraction ratio, A_1/A_T, 1.26; spinner S; equivalent tunnel velocity, 44 m/sec (143 ft/sec).

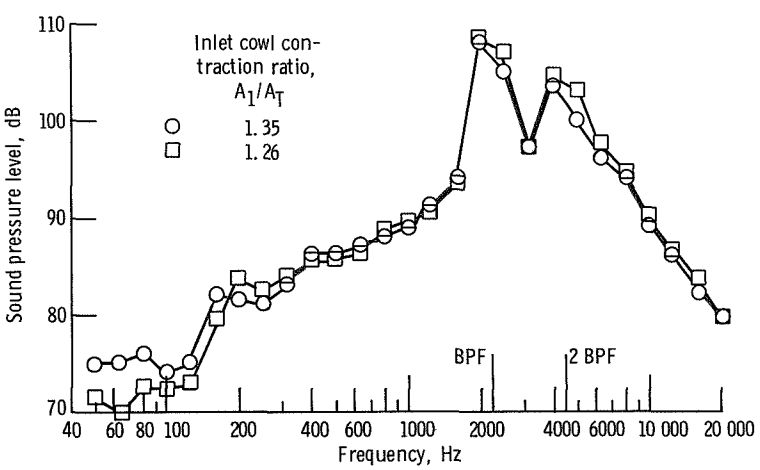

Figure 20. - Noise spectra for two inlets with wind tunnel off. Inlet cowl contraction ratio, A_1/A_T, 1.26 and spinner S; A_1/A_T = 1.35 and spinner L; ratio of fan nozzle exit annulus area to fan duct annulus area, A_e/A_3, 1.11; fan equivalent speed, 120 percent of design.

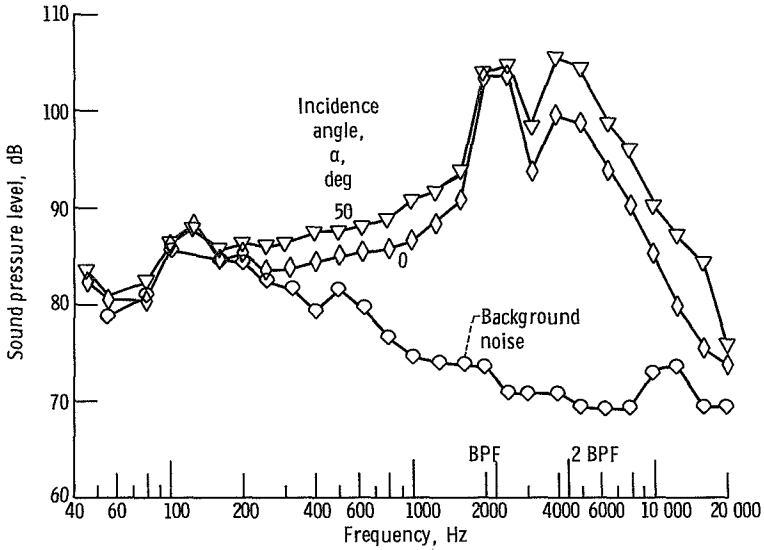

Figure 21. - Noise spectra with inlet cowl contraction ratio A_1/A_T of 1.35 and spinner L. Ratio of fan nozzle exit annulus area to fan duct annulus area, A_e/A_3, 1.11; equivalent tunnel velocity, 44 m/sec (143 ft/sec); fan equivalent speed, 120 percent of design.

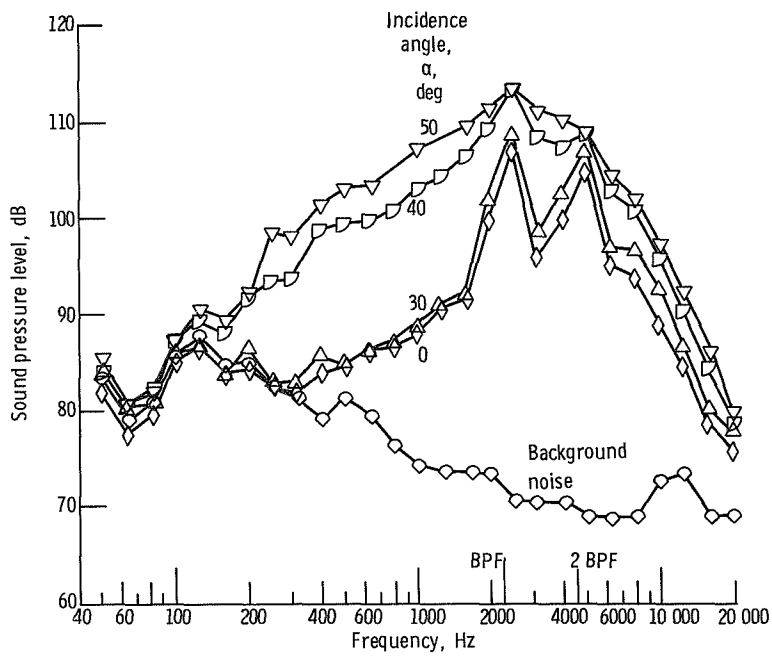

Figure 22. - Noise spectra with inlet cowl contraction ratio A_1/A_T of 1.26 and spinner S. Ratio of fan nozzle exit annulus area to fan duct annulus area, A_e/A_3, 1.11; equivalent tunnel velocity, 44 m/sec (143 ft/sec); fan equivalent speed, 120 percent of design.

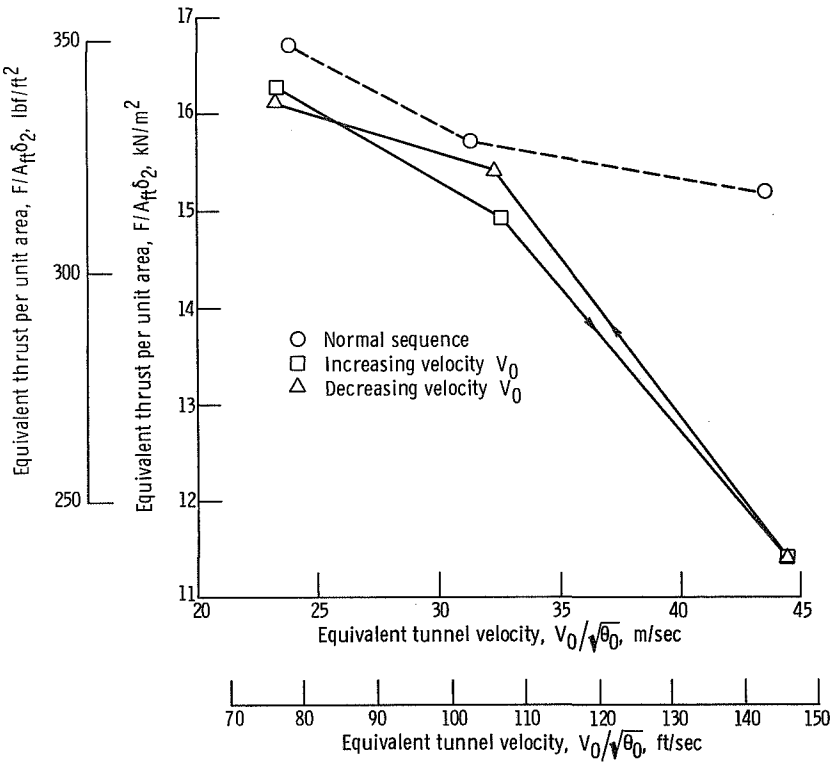

Figure 23. - Effect of variation of test sequence on fan thrust. Incidence angle, α, 50^0; fan equivalent speed, 100 percent of design; inlet cowl contraction ratio, A_1/A_T, 1.35; spinner L; ratio of fan nozzle exit annulus area to fan duct annulus area, A_e/A_3, 1.11.

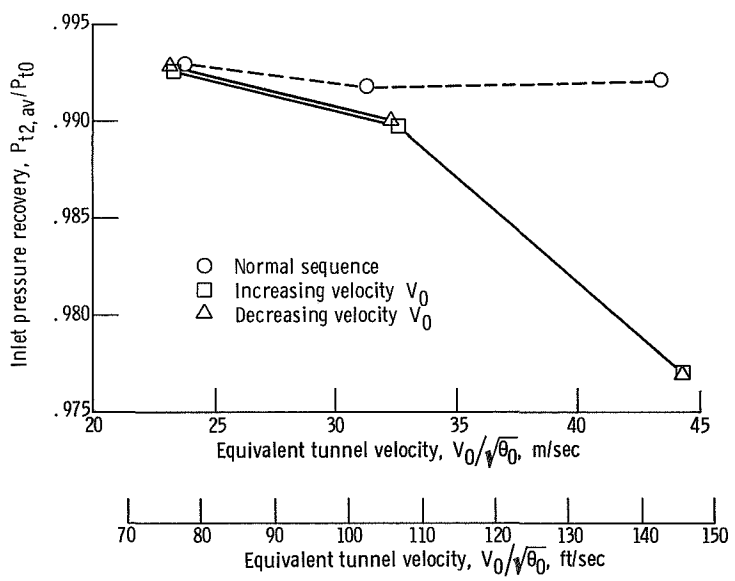

Figure 24. - Effect of variation of test sequence on inlet pressure recovery. Incidence angle, α, 50^0; fan equivalent speed, 100 percent of design; inlet cowl contraction ratio, A_1/A_T, 1.35; spinner L; ratio of fan nozzle exit annulus area to fan duct annulus area, A_e/A_3, 1.11.

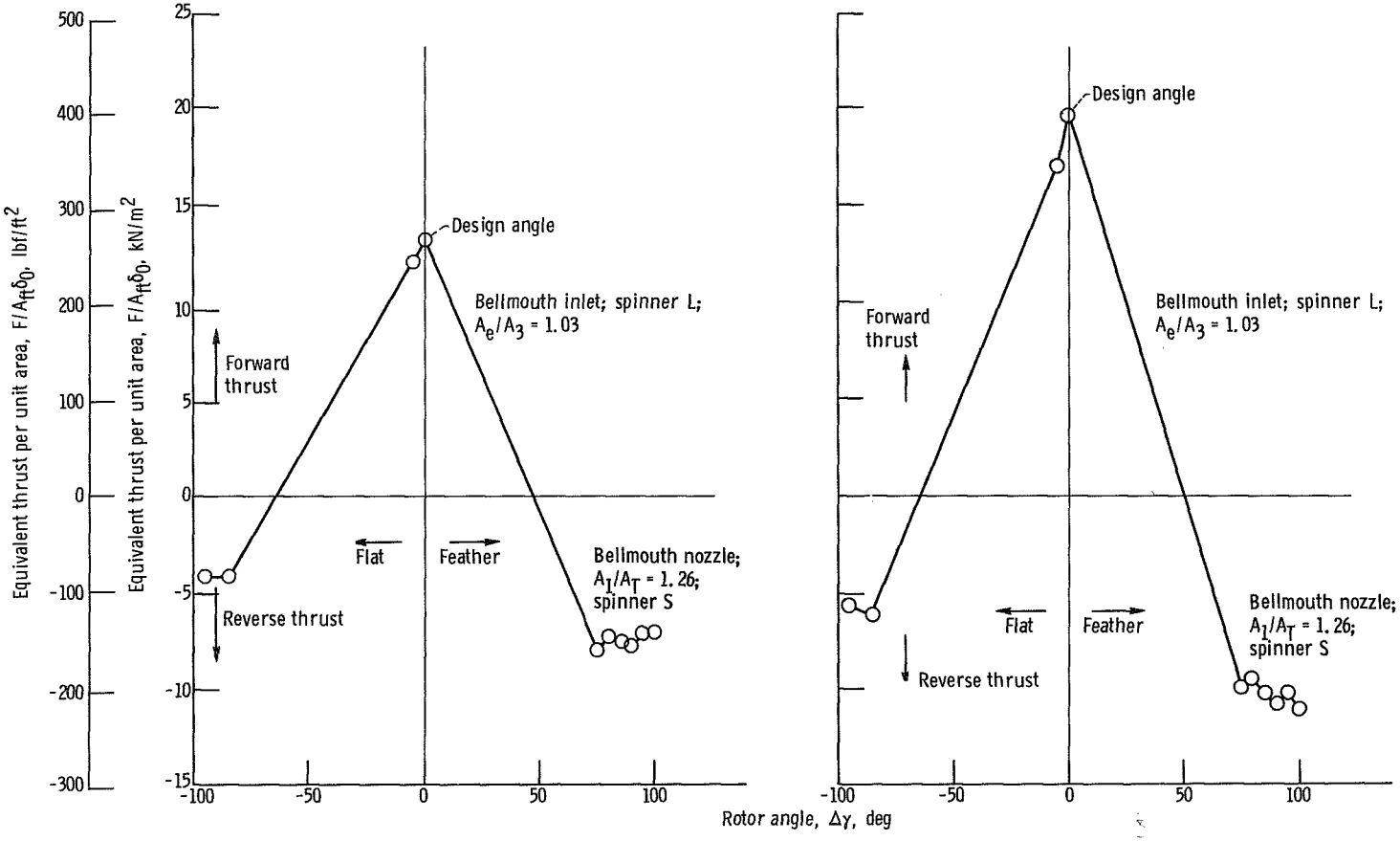

(a) Fan equivalent speed, 90 percent of design.

(b) Fan equivalent speed, 110 percent of design.

Figure 25. - Effect of fan rotor angle on model axial thrust with wind tunnel off.

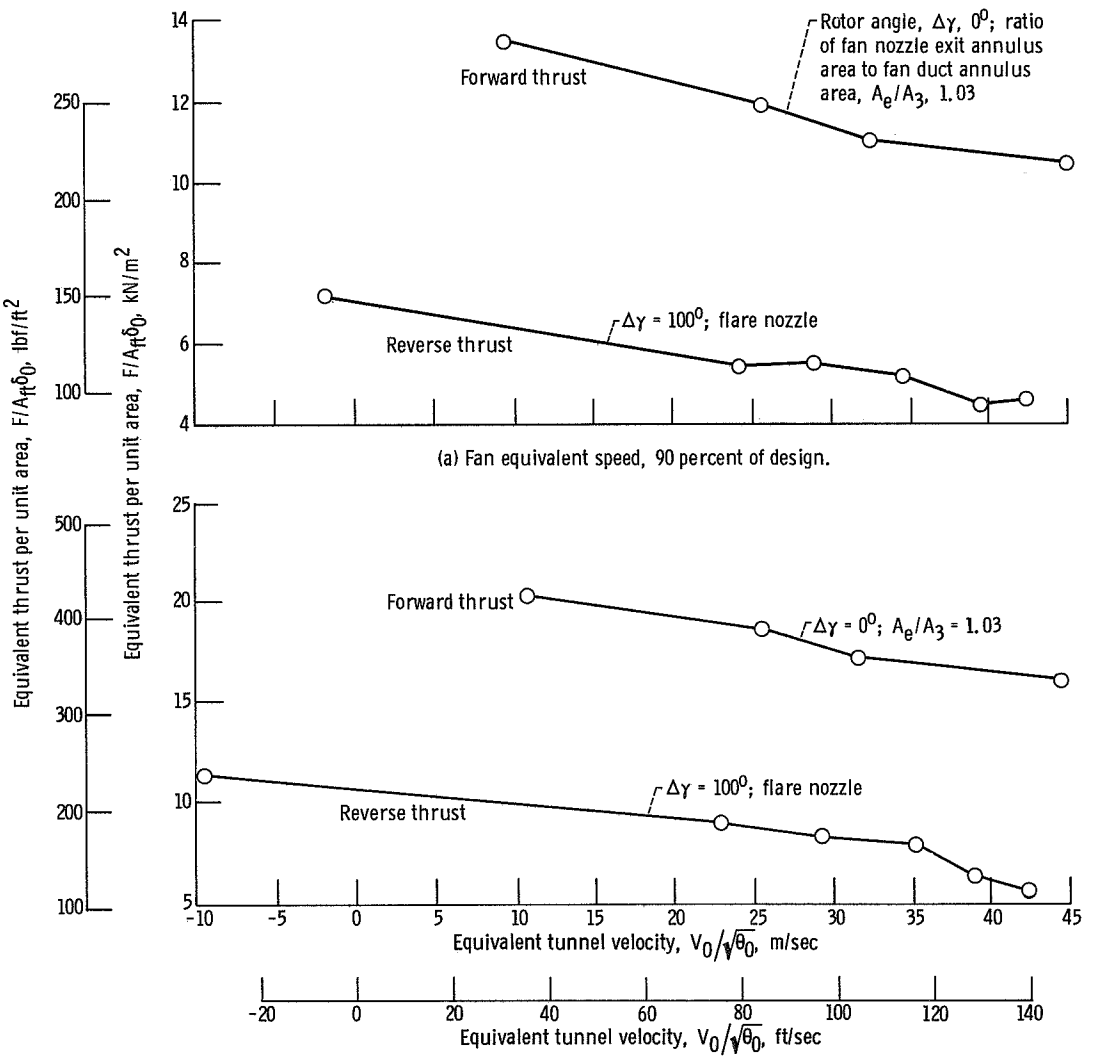

Figure 26. - Effect of tunnel velocity on model thrust. Inlet cowl contraction ratio, A_1/A_T, 1.26; spinner S; incidence angle, α, 10°.

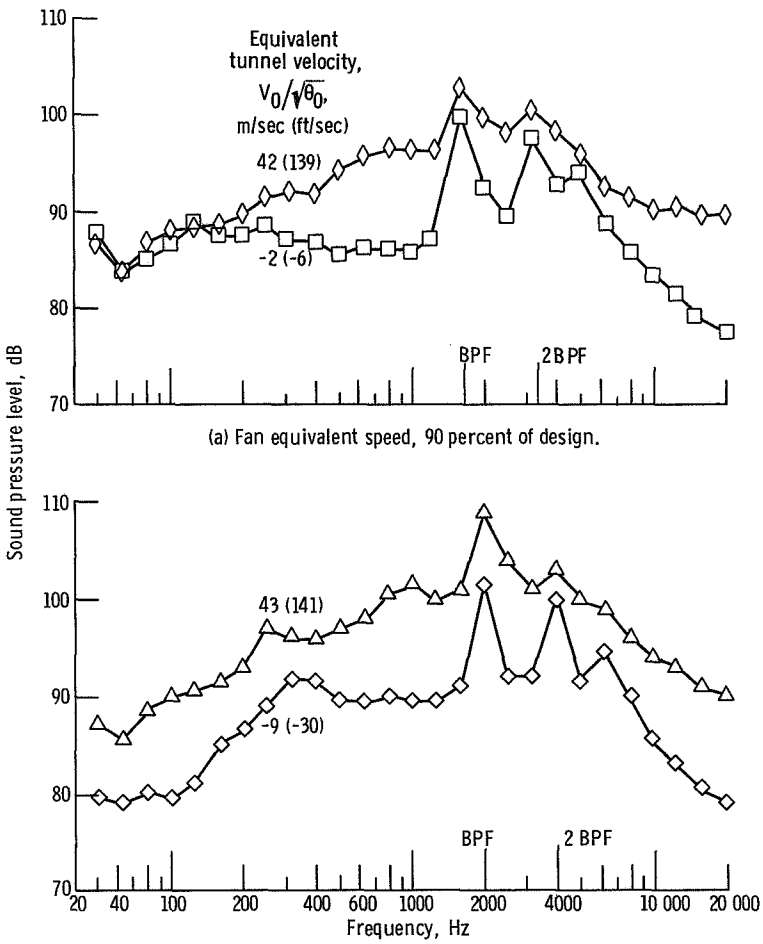

(a) Fan equivalent speed, 90 percent of design.

(b) Fan equivalent speed, 110 percent of design.

Figure 27. - Noise spectra for reverse thrust. Flare nozzle; inlet cowl contraction ratio, A_1/A_T, 1.26; spinner S; rotor angle, $\Delta\gamma$, 100^0; incidence angle, α, 0^0.

NATIONAL AERONAUTICS AND SPACE ADMINISTRATION
WASHINGTON, D.C. 20546

OFFICIAL BUSINESS
PENALTY FOR PRIVATE USE $300

SPECIAL FOURTH-CLASS RATE
BOOK

POSTAGE AND FEES PAID
NATIONAL AERONAUTICS AND
SPACE ADMINISTRATION
451

U.S. MAIL

POSTMASTER If Undeliverable (Section 158 Postal Manual) Do Not Return

"The aeronautical and space activities of the United States shall be conducted so as to contribute . . . to the expansion of human knowledge of phenomena in the atmosphere and space. The Administration shall provide for the widest practicable and appropriate dissemination of information concerning its activities and the results thereof."

—NATIONAL AERONAUTICS AND SPACE ACT OF 1958

NASA SCIENTIFIC AND TECHNICAL PUBLICATIONS

TECHNICAL REPORTS: Scientific and technical information considered important, complete, and a lasting contribution to existing knowledge.

TECHNICAL NOTES: Information less broad in scope but nevertheless of importance as a contribution to existing knowledge.

TECHNICAL MEMORANDUMS: Information receiving limited distribution because of preliminary data, security classification, or other reasons. Also includes conference proceedings with either limited or unlimited distribution.

CONTRACTOR REPORTS: Scientific and technical information generated under a NASA contract or grant and considered an important contribution to existing knowledge.

TECHNICAL TRANSLATIONS: Information published in a foreign language considered to merit NASA distribution in English.

SPECIAL PUBLICATIONS: Information derived from or of value to NASA activities. Publications include final reports of major projects, monographs, data compilations, handbooks, sourcebooks, and special bibliographies.

TECHNOLOGY UTILIZATION PUBLICATIONS: Information on technology used by NASA that may be of particular interest in commercial and other non-aerospace applications. Publications include Tech Briefs, Technology Utilization Reports and Technology Surveys.

Details on the availability of these publications may be obtained from:

SCIENTIFIC AND TECHNICAL INFORMATION OFFICE

NATIONAL AERONAUTICS AND SPACE ADMINISTRATION

Washington, D.C. 20546